Available online at www.sciencedirect.com
ScienceDirect
Journal of Volcanology and Geothermal Research 166 (2007) 47–75
Journal of volcanology and geothermal research
www.elsevier.com/locate/jvolgeores

Magma reservoir failure on the terrestrial planets: Assessing the importance of gravitational loading in simple elastic models

Eric B. Grosfils *

Geology Department, Pomona College, 185 E. Sixth Street, Claremont, CA 91711, United States

Received 17 April 2006; accepted 11 June 2007
Available online 24 July 2007

Abstract

Results from a finite element model characterizing tensile rupture of an internally pressurized ellipsoidal magma reservoir within an axisymmetric elastic half space illustrate that gravity plays a critical role in this process. Failure to incorporate gravitational loading correctly, which is the case for most published models, affects for example: (a) application of corrections designed to account for the presence of the free surface in analytical models; (b) inferences about the internal pressure that a reservoir can sustain prior to rupture; (c) conclusions about the importance of neutral buoyancy, i.e. the relative host rock and magma density structures; and, (d) predictions about the location at which rupture of the reservoir wall will occur and the style of intrusion which will be favored. Analyses that reduce magma reservoirs to a cavity within an unloaded elastic medium, inflated by only an excess pressure component, sacrifice important information and should not be used to interpret reservoir activity or to calibrate more advanced models of volcanic regions and phenomena; an exception to this rule occurs, however, when constraining the pressure that can be inferred from surface displacements for a reservoir of known geometry. In a gravitationally loaded model, the characteristics of the failure process are insensitive to geologically plausible variations in the tensile strength, shear modulus, density structure and gravitational acceleration. As a result the half-space analysis presented here, which will benefit from future expansion to include topography and other factors, can yield insight into not only magma reservoirs on Earth but those thought to have formed within the crusts of Mars, Venus and other solar system bodies as well.

Keywords: magma reservoir; inflation; rupture location; finite element modeling; gravity; gravitational loading; free surface effect; surface displacement; intrusion geometry; neutral buoyancy; planetary volcanism

1. Introduction

Magma reservoirs fed by periodic injections of fresh material ascending from below are a commonly described component of shallow volcanic systems. Repeated infusion of magma into a pre-existing reservoir is one mechanism capable of generating pressures which can induce inflation and eventual fracturing of the surrounding host rock, triggering an intrusive or extrusive volcanic event. Evidence of this process is observed in modern and ancient volcanic systems studied on Earth, for example through inflation and seismicity at Hawaii (Klein et al., 1987), cyclic layering in ancient reservoirs (Turner and Campbell, 1986), laterally extensive dikes composed of multiple injection pulses (Greenough and Hodych, 1990), and radial dike patterns focused on volcanic centers (Muller and Pollard, 1977). In addition, an abundance of intrusive and extrusive volcanic features of probable reservoir origin has been identified on

* Tel.: +1 909 621 8673; fax: +1 909 621 8552.
E-mail address: egrosfils@pomona.edu.

0377-0273/$ - see front matter © 2007 Elsevier B.V. All rights reserved.
doi:10.1016/j.jvolgeores.2007.06.007

Venus (e.g., Head and Wilson, 1992) and Mars (e.g., Wilson and Head, 1994). Attempts to understand the mechanical evolution of magma reservoirs and the factors which govern their failure can therefore provide important insight into how a wide variety of volcanic systems develop and grow on the terrestrial planets.

Complementing field-based research, both analytical and numerical models of pressurized ellipsoidal magma reservoirs have been used extensively to gain insight into magma plumbing systems, surface displacements, eruption styles, and the formation of structural features (e.g., Anderson, 1936; Mogi, 1958; Dieterich and Decker, 1975; Bianchi et al., 1984; Bonafede et al., 1986; Bianchi et al., 1987; McTigue, 1987; Chevallier and Verwoerd, 1988; Gudmundsson, 1988; Dragoni and Magnanensi, 1989; Tait et al., 1989; Bonafede, 1990; Chevallier and Verwoerd, 1990; Quareni, 1990; Sartoris et al., 1990; Parfitt et al., 1993; Chadwick and Dieterich, 1995; Maeda, 2000; Newman et al., 2001; Saunders, 2001; Gudmundsson, 2002; Jellinek and DePaolo, 2003; Trasatti et al., 2003; Lungarini et al., 2005; Trasatti et al., 2005). The majority of the modeling studies performed to date assume an elastic rheology, in some instances adopting it for tractability or convenience and in other cases justifying it on physical grounds. In spite of the seeming simplicity of the elastic approach, however, existing models often identify different parameters as important or unimportant, for instance proximity of the free surface, and thus they incorporate or ignore different factors. As a consequence published modeling results can yield insights that are strongly contradictory (e.g., Sartoris et al., 1990; Parfitt et al., 1993). This is particularly troubling for two reasons. First, modeling of active magmatic systems plays an important role in volcanic hazard identification and assessment. While elastic models clearly can't duplicate the full complexity evident at volcanoes, the potential for gaining critical first-order insights rapidly using elastic models is compromised until existing contradictions between simple elastic models are identified, understood and resolved. Second, as more complex numerical models employing alternate rheologies (e.g., Bonafede et al., 1986; Dragoni and Magnanensi, 1989; Maeda, 2000; Newman et al., 2001; Trasatti et al., 2003, 2005) or other factors are developed to enhance our ability to investigate complex volcanic systems, simple elastic model results are often used for their calibration, with the result that existing problems with simpler models can inadvertently get propagated into more advanced ones. Caution is particularly needed when seeking to understand magma reservoirs on other planets, where model design and evaluation can't be guided by the plethora of datasets (e.g., gravity, seismicity, heat flow, surface tilt) often available to researchers studying active magma systems on Earth.

The goal of the current paper is to provide a framework within which several key differences between existing elastic magma reservoir model results can be explored, compared, and better understood. The main focus is to understand magma reservoir failure and characterize where and under what conditions rupture of the wall will occur. The analysis begins with development and component by component testing of an isotropic and homogeneous half-space model which incorporates all major geological and geometrical factors identified by previous authors. This model is then used to characterize the extent to which magma reservoir failure is sensitive to different geological and geometrical parameters. Finally, based on this analysis, several key issues are assessed, including (a) implementation of depth-dependent host rock stress states, (b) failure location and intrusion style, (c) vertical displacement at the surface and inferences about subsurface magma pressures, (d) the magma pressure required to initiate rupture, (e) uniaxial strain conditions, and (f) the formation of radiating dike swarms. Throughout this paper the focus is on reservoirs subjected to physical conditions appropriate for Earth and Mars, but the latter is explored only to the extent necessary to elucidate fundamental behaviors. It is important to note that the current framework is intended as neither an endorsement of elastic model suitability for modeling magma reservoir processes nor a rejection of such an approach. Elastic models have value in some circumstances, for instance when rapid or first order insight into a magma plumbing system is required on the basis of limited observational data (e.g., Bianchi et al., 1984), and not in others, for instance investigation of long-lived systems better characterized by viscoelastic behavior or another rheological response (e.g., Newman et al., 2001). However, to the extent that a magma reservoir can be characterized as an internally pressurized ellipsoid subject to tensile failure within an elastic host, the model results presented here can be used to gain direct insight into failure conditions and related phenomena.

2. Computational model

2.1. Model formulation

COMSOL Multiphysics software (http://www.comsol.com/) is used to develop axisymmetric finite element models (FEMs) which treat the reservoir as an internally pressurized ellipsoid within an elastic host in the absence

of remote tectonic stresses. Each model mesh contains in excess of 15,000 elements, and a sample mesh, in this case depicting a spherical reservoir 1 km in radius centered 15 km below the surface, is shown in Fig. 1a. The left hand boundary of the cylindrical mesh ($r=0$) is free to displace in the vertical direction, and defines the vertical rotation axis of the axisymmetric system. The lower boundary ($z=-30$ km) is free to displace in the horizontal direction, the right hand boundary ($r=30$ km) is free to move in the vertical direction, and the upper boundary ($z=0$) is

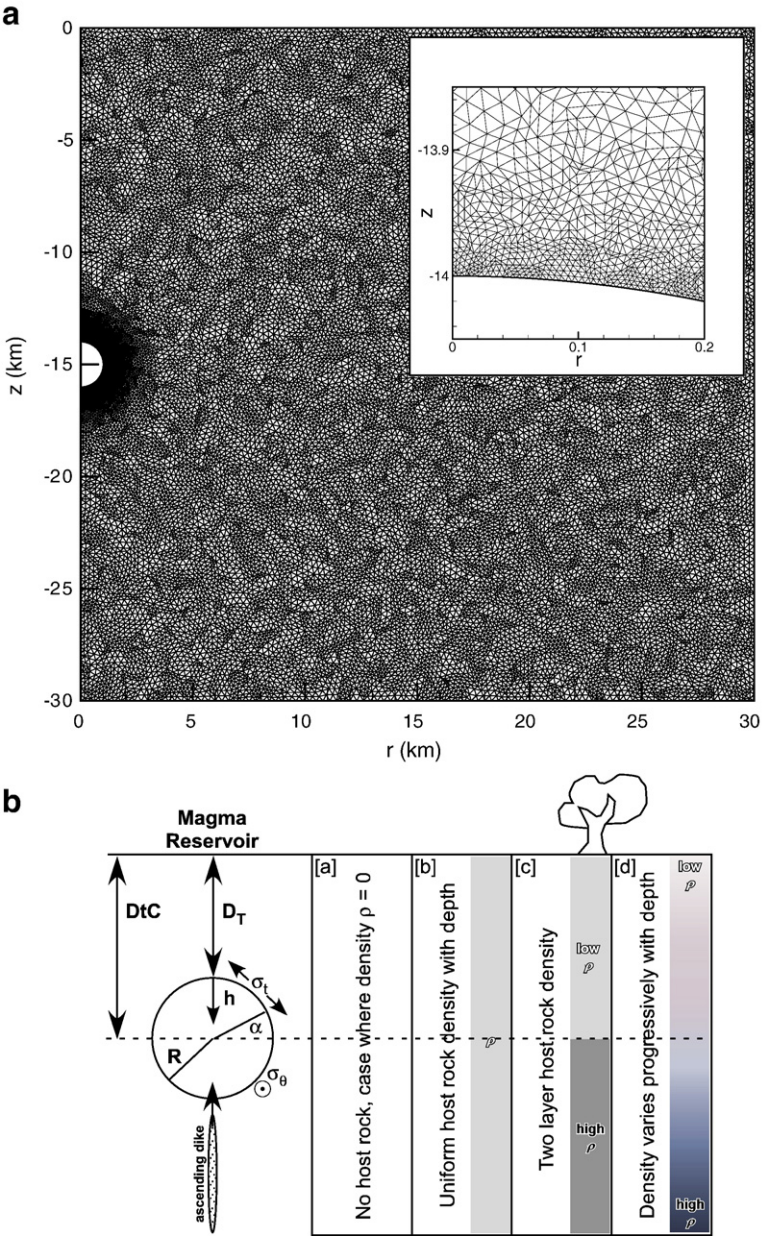

Fig. 1. Model conditions. (a) Sample of an axisymmetric finite element mesh employed during the current study; to minimize potential edge effects, the region studied in any given model was never less than 30 km wide by 20 km deep. The left hand side is the axis of rotation, the bottom is free to displace in the radial direction with the vertical displacement fixed at zero, the right hand side is free to displace in the vertical direction with the radial displacement fixed at zero, and the upper surface is otherwise left free of displacement constraints. Internal stresses applied normal to the reservoir wall are described by Eq. (4). A typical mesh has in excess of 15,000 elements, with more than 1000 used to define the reservoir wall (see inset). (b) Schematic depiction of the host rock density structures and key magma reservoir model parameters explored. The wall-parallel stresses include σ_t, tangential to the reservoir wall within the plane of the page, and σ_θ, tangential to the wall and perpendicular to the page.

otherwise free of displacement constraints. An initial reference state of stress (e.g., lithostatic) is imposed throughout the host rock, and each element is loaded with an internal body load per unit volume ρg, where ρ is the density of the host rock at a given depth and g is the gravitational acceleration. In response to the host rock stresses and those applied to the interior reservoir wall (discussed below), the model calculates stresses (σ_r, σ_z, σ_θ, σ_{rz}; compression negative) throughout the volume in polar cylindrical coordinates. From these, it is straightforward to determine the stresses normal and parallel to the reservoir walls at any given location. The circumferential (hoop) stress σ_θ (Fig. 1b) is obtained directly from the finite element solution, while the stresses normal and tangential to the reservoir wall are calculated from the remaining finite element stresses such that

$$\sigma_R = \sigma_r \cos^2\alpha + \sigma_z \sin^2\alpha + \sigma_{rz} \sin 2\alpha \quad (1)$$

$$\sigma_t = \sigma_r \sin^2\alpha + \sigma_z \cos^2\alpha - \sigma_{rz} \sin 2\alpha \quad (2)$$

where σ_r, σ_z and σ_{rz} are the radial, vertical and shear stresses, and α is the angle in degrees between the horizontal and a line connecting the center of the reservoir to a point in space, given for a spherical reservoir by

$$\alpha = 90 - \cos^{-1}\left(1 - \frac{h}{R}\right) \quad (3)$$

where h is the depth below the reservoir crest at which failure occurs and R is the reservoir radius. The condition adopted for failure and intrusion to occur is that either the circumferential or tangential stress in an element adjacent to the reservoir wall (Fig. 1) must exceed the tensile strength of the rock, which for typical crustal material is on the order of 0–10 MPa (e.g., Schultz, 1995).

A very high density of elements is employed near the reservoir, permitting careful examination of the stresses critical to failure in this region (Fig. 1a, inset). The reservoir wall is defined over 180° of arc by approximately 1000 elements. For a reservoir with R=1 km, each bounding element is a few meters across, promoting precise determination of the location along the wall at which tensile failure will preferentially take place.

Boundary conditions are applied to the interior of the reservoir wall to reflect the stresses produced by the magma they confine. These magma-generated stresses are assumed to act normal to the reservoir boundary. The total pressure P_m applied by the magma is the sum of two components, so that

$$P_m = P + \rho_m g h. \quad (4)$$

The first term is the reservoir pressure P, which acts uniformly upon all parts of the reservoir wall and could incorporate, for instance, a component reflecting injection of new magma into the reservoir. The second term is the weight of the magma, which for a magma of density ρ_m varies with depth h below the roof of the reservoir (we follow other authors in defining h as positive downwards); subsequent analysis and discussion will show that magma density variations play an almost negligible role in the determination of the point of failure even at geologically extreme density values, and hence more subtle configurations, such as the two-layer magma reservoir density systems introduced by other authors (e.g., Parfitt et al., 1993), are not explored. Given the depth dependence of the second term in Eq. (4), the normal stress P_m applied to the interior of the reservoir wall increases steadily with depth h.

2.2. Host rock stress state

In many geologic situations it has been demonstrated that a lithostatic stress state in the host may be the most reasonable to consider as a reference (e.g., McGarr, 1988), where the horizontal radial and circumferential stresses are equal to the vertical stress, i.e.

$$\sigma_r = \sigma_\theta = \sigma_z. \quad (5)$$

This stress state is the one most commonly assumed in quantitative modeling efforts which investigate magma reservoir behavior. An alternate stress state sometimes used in numerical models, however, is that generated in response to vertical uniaxial strain. This may be appropriate, for instance, if a layer of rock formed at the surface is subsequently buried rapidly, subjecting it to a vertical load while effectively inhibiting lateral displacement at large distances. For a body of rock with a Poisson's ratio ν=0.25, the horizontal stresses generated in response to uniaxial strain are one-third of the vertical stress, so that

$$\sigma_r = \sigma_\theta = \frac{\sigma_z}{3}. \quad (6)$$

In either reference state, the vertical stress in the host rock is given by

$$\sigma_z = \rho_r g z \quad (7)$$

where the density of the rock ρ_r can vary with z, the depth below the surface. To retain flexibility and facilitate comparison with previous models, both host rock stress states are considered in order to understand how this difference contributes to failure of the reservoir wall and the style of volcanism which potentially results.

2.3. Model assessment

To assess the accuracy of the finite element calculations and ensure that the geometry and mesh adopted yield sufficient sensitivity for a failure analysis, different components of the system were compared carefully with analytical benchmarks.

First, to verify that the host rock loading conditions indeed create the desired state of vertical stress, FEM-calculated values of σ_z taken from a vertical cross section

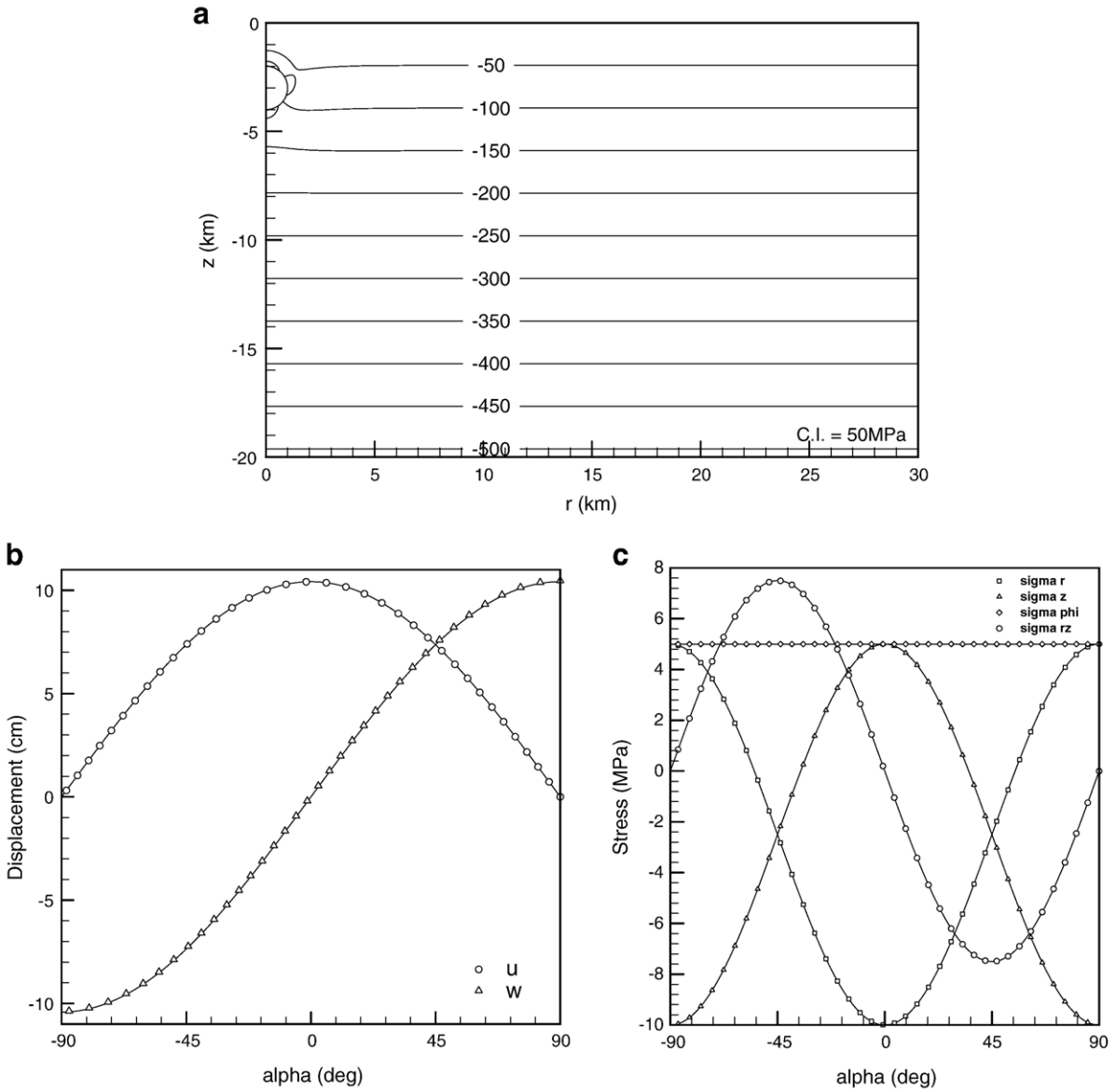

Fig. 2. Test of host rock and magma reservoir stress implementation. (a) Sample contour plot, for σ_z in a uniform host case, demonstrating the absence of regional edge effects and that the model size is sufficient to prevent edge effects from affecting the stress perturbation calculation around the reservoir. (b and c) Displacement and stress tests for a reservoir of radius $R=1$ km, far from the free surface (DtC=15 km), in the absence of gravitational stresses (i.e., $g=0$ m s^{-2}). This reduces the model to a pressurized sphere in an unloaded elastic half space, and permits comparison with analytical results for an infinite space; $P=10$ MPa. (b) Displacements u and w in the r- and z-directions for the reservoir-adjacent elements. Alpha is the angle from horizontal, with $\alpha=90°$ the top pole of the reservoir and $\alpha=-90°$ the bottom. Thin lines show analytical predictions, while the symbols show the results of the FEM calculation. The maximum differences observed at the wall of the reservoir are a few hundredths of a millimeter, and those for the full 30 km by 30 km section are only a few tenths of a millimeter. (c) Analytically predicted (lines) and calculated (symbols) stress values, in polar cylindrical coordinates, at the reservoir wall. Maximum differences observed are <2 kPa for all four stresses calculated directly by the FEM.

(at $r=15$ km in a 30 km wide by 20 km deep model) were compared with analytically predicted values (i.e., Eq. (7)). The maximum absolute difference between predicted and calculated stresses of $\sim 6\times10^{-3}$ MPa, an error at this location of 0.004%, indicates that the desired vertical load is implemented correctly. Identical tests, performed to verify that the FEM-calculated horizontal stresses also accurately reflect either the lithostatic stress or uniaxial strain conditions desired, yield similar results, as did tests using the other host rock density configurations explored further below. The magma loading term was also tested as a function of depth h, with maximum absolute differences between predicted and calculated stresses less than $\sim 1\times10^{-5}$ MPa, yielding a percentage error at this location of 5×10^{-5}.

Second, Fig. 2a shows σ_z contours for a lithostatic test model run. All contour lines are horizontal throughout the cross section, except of course in the vicinity of the reservoir where perturbations to the host rock stress are induced. This demonstrates that no significant edge effects affect the host rock stress throughout the volume studied. In addition, quantitative testing was performed

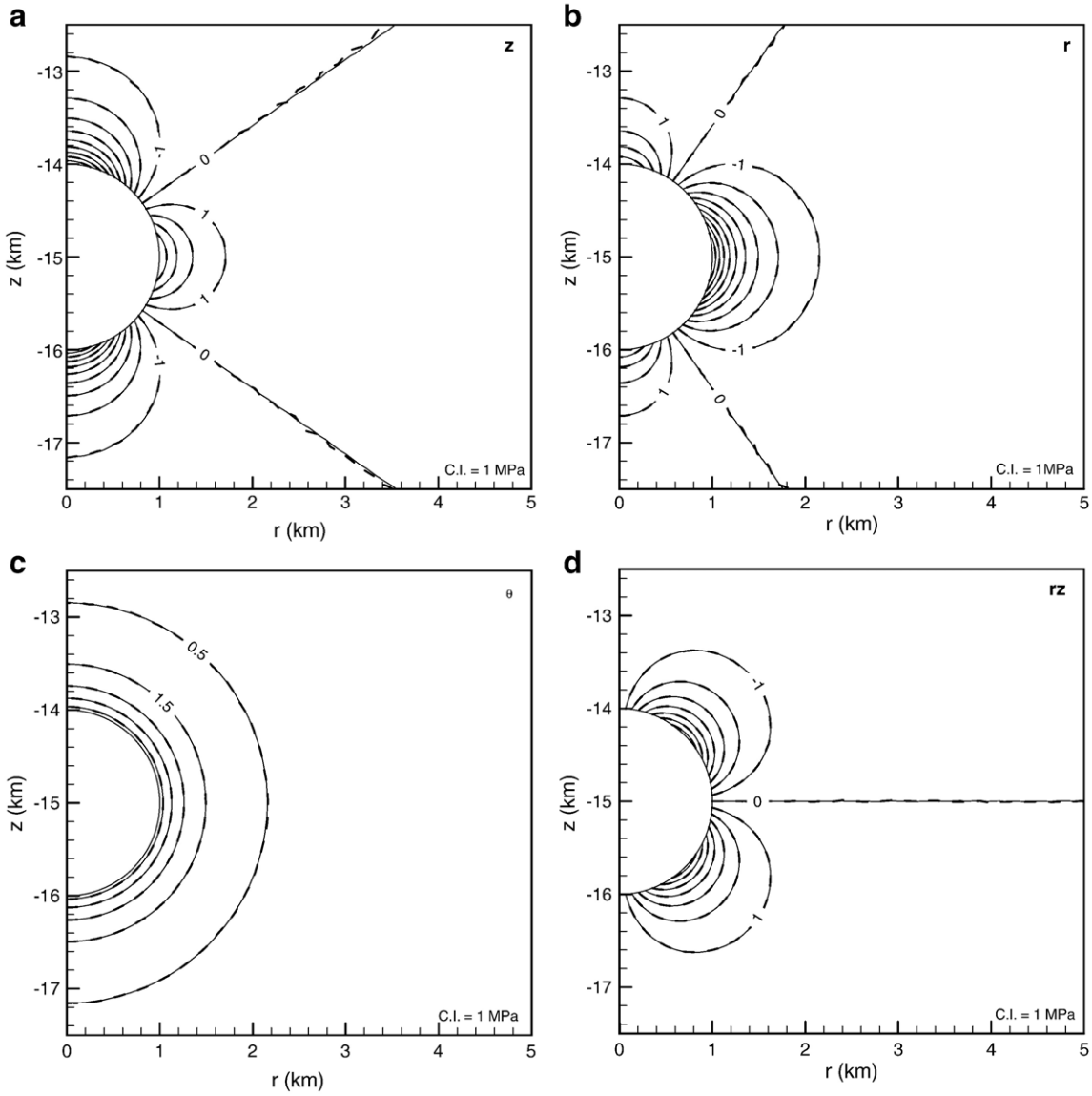

Fig. 3. Near-reservoir stress plots, for a reservoir of radius $R=1$ km, far from the free surface (DtC=15 km), in the absence of gravitational stresses. The thin line is the analytical model prediction, the thick dashed line is the FEM calculation result. Maximum differences observed across a full 30 km by 30 km section are on the order of ~10 kPa for all stresses examined. (a) σ_z. (b) σ_r. (c) σ_θ. (d) σ_{rz}.

to verify that the region used for any given model run was of sufficient size to prevent the stress perturbations of interest, introduced by the presence of the reservoir, from being affected by the proximity of the subsurface boundaries of the mesh.

As a third test, since it is very important to ensure that stress and displacement calculations yield accurate results in the immediate vicinity of the reservoir, a 1 km radius magma chamber was placed far from the free surface (15 km depth) and the gravity value g was set to zero to eliminate gravitational stress components. Under these conditions, the reservoir approximates a uniformly pressurized sphere in an infinite elastic medium, and both the displacement of the walls of the sphere and the magnitude of the resultant stresses can be calculated analytically at any point in the surrounding material (e.g., Timoshenko and Goodier, 1951). Given a uniform pressure P within the reservoir, displacements in the r- and z-directions are predicted analytically by

$$u = \frac{PR^3 r}{4G(r^2+z^2)^{3/2}} \tag{8}$$

$$w = \frac{PR^3 z}{4G(r^2+z^2)^{3/2}} \tag{9}$$

where G is the shear modulus, R is again the reservoir's radius, and r and z are the horizontal and vertical coordinates of a point relative to the center of the reservoir. Similarly, within the surrounding material the stresses normal and tangential to the wall of a uniformly pressurized reservoir are predicted analytically by

$$\sigma_R = -P\left(\frac{R}{\sqrt{r^2+z^2}}\right)^3 \tag{10}$$

$$\sigma_T = -\frac{\sigma_R}{2} = \frac{P}{2}\left(\frac{R}{\sqrt{r^2+z^2}}\right)^3. \tag{11}$$

These analytical stress and displacement predictions are compared with the results from the finite element model calculations. Using $P=10$ MPa, displacements in the horizontal and vertical directions closely approximate the analytical results (Fig. 2b). For the ~1000 elements which define the reservoir wall, the differences observed between the FEM and analytical predictions are everywhere less than 5×10^{-4} m (0.5% error at the maximum difference location) for the z-displacement and less than 1.5×10^{-5} m (0.01% error at this location) for the r-displacement. An analogous level of agreement is also seen when the finite element and analytical stresses are compared (Fig. 2c), where the analytical stresses from Eqs. (10) and (11), translated into cylindrical coordinates, are given by

$$\sigma_r = \sigma_R\cos^2\alpha + \sigma_T\sin^2\alpha \tag{12}$$

$$\sigma_z = \sigma_R\sin^2\alpha + \sigma_T\cos^2\alpha \tag{13}$$

$$\sigma_\theta = \sigma_T \tag{14}$$

$$\sigma_{rz} = (\sigma_R - \sigma_T)\sin\alpha\cos\alpha. \tag{15}$$

The maximum difference observed between predicted and FEM-calculated stresses at the reservoir wall is $\sim3.7\times10^{-3}$ MPa, yielding an error at this location of 0.04%. Results for a broader region surrounding the reservoir are shown in Fig. 3. It is clear from the contours shown that the stresses derived from the finite element model continue to approximate the analytical solution closely away from the reservoir wall. Together, the results from Figs. 2 and 3 demonstrate that the different components of the finite element model possess sufficient

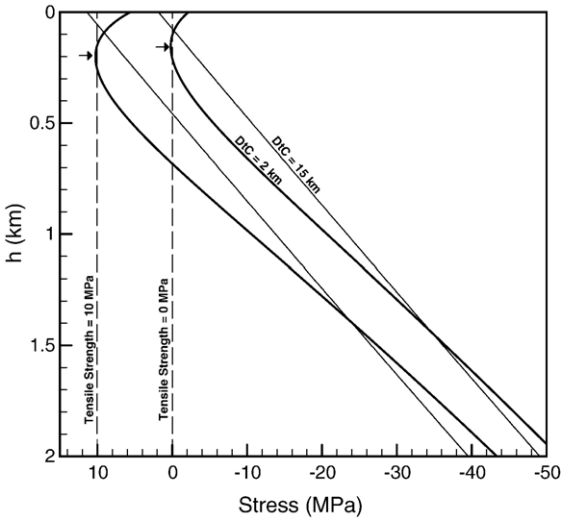

Fig. 4. Illustration of initial failure determination, for $T=0$ MPa and 10 MPa and reservoirs with $R=1$ km centered at DtC of 2 km (near-surface) and 15 km (deeply seated). The host rock stress is lithostatic, the density structure is uniform with depth, and $\rho_r=\rho_m=2600$ kg m^{-3}. Pressure P is increased until one of the tangential stresses exceeds the tensile strength value. For the DtC=15 km case (thin lines), $\sigma_t\approx\sigma_\theta$ (only σ_t is plotted) and first failure occurs at $h=0$ km, the crest of the reservoir. When DtC=2 km (heavy lines), σ_t first exceeds the tensile strength T, and the curvature exhibited reflects the influence of the free surface. The depth of failure h below the roof of the reservoir, marked by arrows, differs by only about 50 m when the tensile strength is varied. For a geologically plausible range of values, T plays only a minimal role in determining the failure location.

accuracy to permit careful examination of the stresses adjacent to an ellipsoidal magma reservoir. By extension, the model can be used with confidence to investigate the conditions that dictate where and under what conditions initial tensile failure of a magma reservoir's wall will occur.

2.4. Model parameters and approach

In order to characterize the location at which tensile failure of the magma reservoir wall will occur under different conditions, several hundred models were run. The parameters assessed include: reservoir shape (spherical, prolate, oblate), volume, depth and uniform internal pressure P; magma and host rock density structure with depth (uniform, two layer, and smoothly increasing; see Fig. 1b); gravity; and, host rock stress state conditions (lithostatic, uniaxial strain).

Procedurally, for any given combination of geological and geometric parameters examined the pressure P is iterated until the value required to induce initial tensile failure of the reservoir wall is identified (Fig. 4); in practice the iterations explore P in terms of multiples of σ_z (to two decimal places) at the depth of the reservoir's center. Tensile failure occurs when and where σ_t or σ_θ first exceeds the tensile strength of the rock, which will also control the initial style favored for the resultant intrusion (e.g., lateral sill or dike). For simplicity the tensile strength used to identify the point of failure is $T=0$ MPa, because the actual value selected has only a minimal effect upon the failure location even in the most extreme cases (Fig. 4).

Throughout the modeling performed, unless otherwise noted, Poisson's ratio $\nu=0.25$ and Young's Modulus $E=60$ GPa, translating into a shear modulus $G=E/(2*(1+\nu))=24$ GPa. The value for E (or G) employed is commensurate with values employed in some studies but stiffer than the values used in others (e.g., Newman et al., 2001; Gudmundsson, 2002); tests performed, however, indicate that the location of magma reservoir failure is insensitive to the value of E employed for the range of values commonly used in the literature (i.e., ~1–100 GPa). This insensitivity does not apply to surface displacement calculations, however, since displacement will be amplified as G decreases (e.g., Mogi, 1958).

3. Results

3.1. Sphere, uniform host rock density

3.1.1. Lithostatic conditions

The simplest situation to consider is a deeply buried (to eliminate surface effects) spherical reservoir where the magma (ρ_m) and host rock (ρ_r) densities are identical

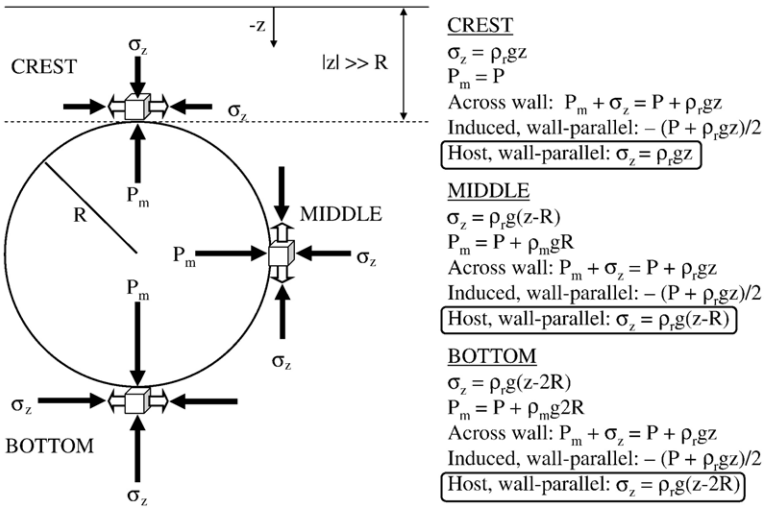

Fig. 5. Conceptual illustration of model under lithostatic conditions when $\rho_r=\rho_m$ and the depth of the reservoir is much greater than the radius to eliminate effects caused by the proximity of the free surface; z is negative downward. Under these conditions the balance of magma and host rock stresses across the reservoir wall is depth-invariant, and the wall-parallel extensional stresses induced (white arrows) as a result are depth-invariant as well. The wall-parallel component of the lithostatic stress, however, increases with depth. Since both the tensile strength of the rock and the wall-parallel extensional stresses induced by the normal stress balance across the wall are invariant with depth, the depth-dependent variation in the wall-parallel component of the lithostatic stress in the host rock will dictate the failure location. As the uniform component of the magma pressure, P, is increased, this means that rupture of the reservoir wall will first occur at the crest of the chamber, where the magnitude of the wall-parallel component of the host rock stress resisting failure is smallest.

(Fig. 5). Under these conditions, breaking the full problem into two separated components makes it straightforward to predict where failure should occur via a simple thought experiment. The first component is the wall-normal stress balance driving radial displacement, a process which induces wall-parallel stresses. At the crest of the chamber, where $h=0$, the magma pressure P_m is simply P (see Eq. (4)), and the normal stress balance $P_m+\rho_r gz$ (z negative) across the reservoir wall is simply $P+\rho_r gz$; the reservoir wall is in a state of equilibrium when this balance is zero, and it will tend to expand outward or collapse inward as the balance grows increasingly positive or negative. Because the magma and host rock densities are set equal, the increase in P_m with depth (at the center of the reservoir for example, where $h=R$, $P_m=P+\rho_m gR$) is matched by the increase in the weight of the host rock (i.e., at this location $\rho_r g(z-R)$), with the result that the normal stress balance remains $P+\rho_r gz$ at any depth h below the crest. As P increases in magnitude and drives outward expansion, tangential extension is induced; in this specific set of physical circumstances (i.e., far from the surface, no variance in wall-normal stress balance) Eq. (11) dictates that the induced tension will be of equal magnitude at all locations, meaning that failure is equally likely at any depth once the tensile strength of the rock is exceeded. The second component of the problem, neglected thus far, is the wall-parallel component of the host rock lithostatic stress, which increases with depth. When both components of the problem are considered together, it is clear that initial rupture should occur where the tension induced by outward expansion of the reservoir first overcomes the combination of the tensile strength and the wall-parallel lithostatic stress. Initial failure should thus occur at the crest of the reservoir.

In practice, geologically plausible variations in magma density relative to the surrounding host will cause the normal stress balance to become depth-dependent. The lithostatic stress variation in the host rock will continue to dominate the failure location, however, since the magnitude of the variation from crest to base, $|\rho_r g2R|$, will normally be significantly greater than the magnitude of the stress change induced by the host-magma density difference, given by $|(\rho_m-\rho_r)g2R|$. Even when extreme differences in host rock and magma densities are considered this remains true, as demonstrated in Fig. 6.

Fig. 7a demonstrates how the failure location varies for reservoirs with radii R of 0.5 and 1.0 km under lithostatic conditions. As the depth of a reservoir decreases, failure

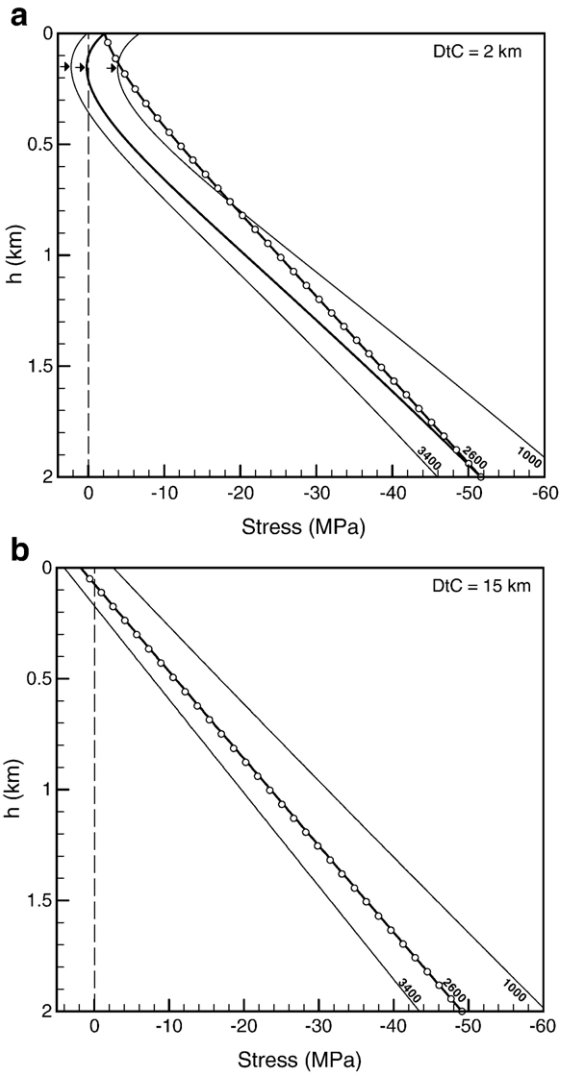

Fig. 6. Role of density contrasts in failure location determination. For a uniform density host rock of $\rho_r=2600$ kg m^{-3}, lithostatic stress conditions, and $R=1$ km, curves for magmas of density $\rho_m=1000$, 2600 and 3400 kg m^{-3} are shown. Results are in essence unchanged for two layer and smoothly varying host rock density configurations (not shown). The stress σ_t is plotted in all cases, and σ_θ for the $\rho_m=2600$ kg m^{-3} case is also plotted (circles). (a) When DtC=2 km, σ_t is more tensile than σ_θ, thus failing first, and P is held constant to illustrate the effect of the density difference. When $\rho_m=1000$ kg m^{-3}, the contribution of magma weight $\rho_m gh$ to the normal stress is less than when $\rho_m=2600$ kg m^{-3}, and thus the pressure P required to induce failure (i.e., to shift the curve left until it crosses the $T=0$ MPa location shown by dashed line) must be greater to compensate. The inverse is true for the $\rho_m=3400$ kg m^{-3} case. For magma density variations that cover a generous range of plausible values, the location of first failure (arrows) differs by ~10 m, demonstrating that magma density does not affect failure location. (b) For DtC=15 km, the location of first failure remains pinned to the upper pole of the reservoir. As magma density decreases the pressure must again be higher to compensate. The $\rho_m=2600$ kg m^{-3} case illustrates that the two tangential stresses are essentially equivalent, promoting vertical dikes of any orientation.

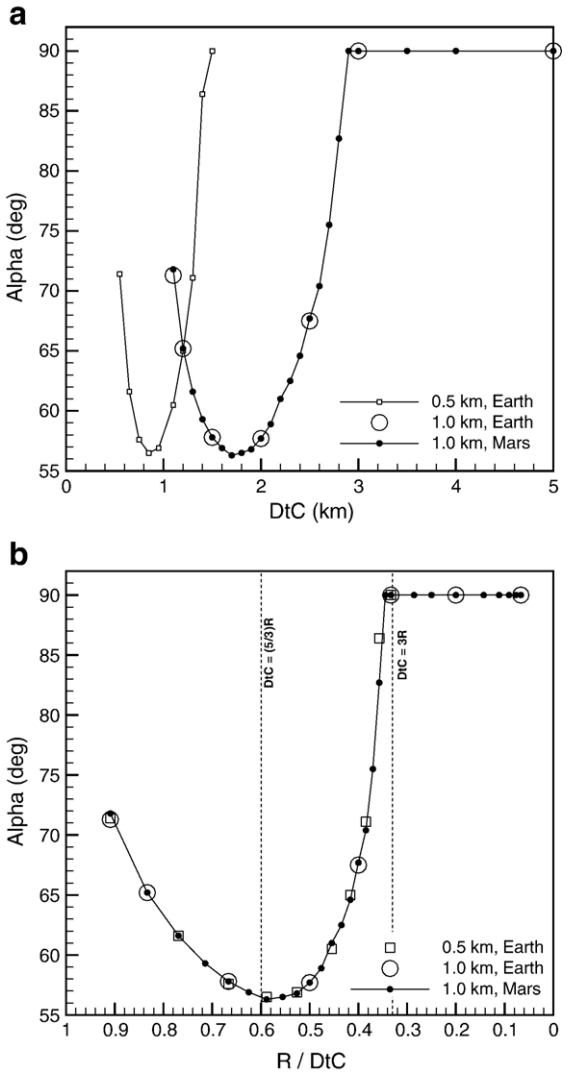

Fig. 7. Failure location as a function of DtC for a spherical reservoir subjected to lithostatic stress when $\rho_m = \rho_r$ and the host rock density is uniform with depth. (a) The location of failure at any given DtC for any given radius R is independent of the value of g selected, and for any given DtC the failure location is dependent upon R. (b) The location of failure, α, is a function of R/DtC. When $\mathrm{DtC} \geq 3R$ failure occurs at the crest of the reservoir. At shallower depths, the location of failure rotates away from the crest, reaching a minimum of ~56° when $\mathrm{DtC} \approx (5/3)R$. The stress σ_t first exceeds the tensile strength T in all instances, and thus failure of a deep-seated reservoir promotes vertical dike injection while failure at shallower depths favors circumferential intrusion.

occurs consistently at the crest of the reservoir until it reaches shallow depths. Once the reservoir begins to 'feel' the surface, allowing greater vertical displacements of the wall across the upper half of the reservoir, the asymmetry of the strain that occurs causes the failure location to rotate away from the crest (see Section 4.4), reaching a maximum rotation angle (maximum depth) of $\alpha \approx 56°$ ($h \approx 170$ m when $R = 1$ km) before rotating back toward the peak. When failure occurs at the crest of the reservoir, $\sigma_t = \sigma_\theta$ and hence vertical dikes of any strike can occur. When failure happens away from the crest, however, $\sigma_t > \sigma_\theta$ (i.e., σ_t is more tensile than σ_θ) and hence the resultant intrusion style favored is circumferential, possibly conducive to the formation of ring dikes or cone sheets as α decreases. Fig. 7b demonstrates the scale-independence of the failure location behavior, which has been noted by other authors (e.g., McTigue, 1987), and also shows that it is not dependent upon the non-zero value of g selected. Based on the models presented here, the surface effect begins to affect the failure location when the depth to the reservoir center (DtC) is three times the reservoir radius, and the maximum rotation angle occurs when $\mathrm{DtC} \approx (5/3)R$.

3.1.2. Uniaxial strain conditions

Unlike the lithostatic case, identifying where a reservoir deeply buried within a host subjected to uniaxial strain conditions will fail is not conceptually straightforward to predict. At the crest and bottom of the reservoir, the outwardly-directed magma pressure P_m is applied against the vertical component of the lithostatic stress, σ_z, while rupture of the host is resisted by T and by wall-parallel host rock stresses only one-third the magnitude of the vertical stress. At the midpoint of the reservoir, P_m has increased in magnitude by an amount $\rho_m g R$ and the vertical stress in the host rock has changed by the same margin, assuming again that $\rho_m = \rho_r$. However, the outward-directed magma pressure P_m, under uniaxial strain conditions, works against a horizontal stress that is only one-third the magnitude of σ_z, and rupture of the rock is resisted by T as well as (a) host rock stresses of magnitude $\sigma_z/3$ in a horizontal plane, and (b) host rock stresses of magnitude σ_z in a vertical plane. This means that tensile failure leading to lateral dike injection will be highly favored over lateral sill injection at the midpoint of the reservoir if tensile failure first occurs at this depth.

Fig. 8 shows an example of how the magnitudes of σ_t and σ_θ vary as a function of position around the margins of a magma reservoir subjected to uniaxial conditions. As expected, the magnitudes of σ_t and σ_θ are equivalent at the crest and bottom of the reservoir, while at the midpoint of the reservoir σ_θ is everywhere more positive (more tensile) than σ_t. Whether the reservoir is located at great or shallow depth, failure at the poles of the reservoir is clearly favored, in agreement with results reported previously (e.g., Sartoris et al., 1990). Mathematically, failure will consistently occur at the bottom pole; however, the

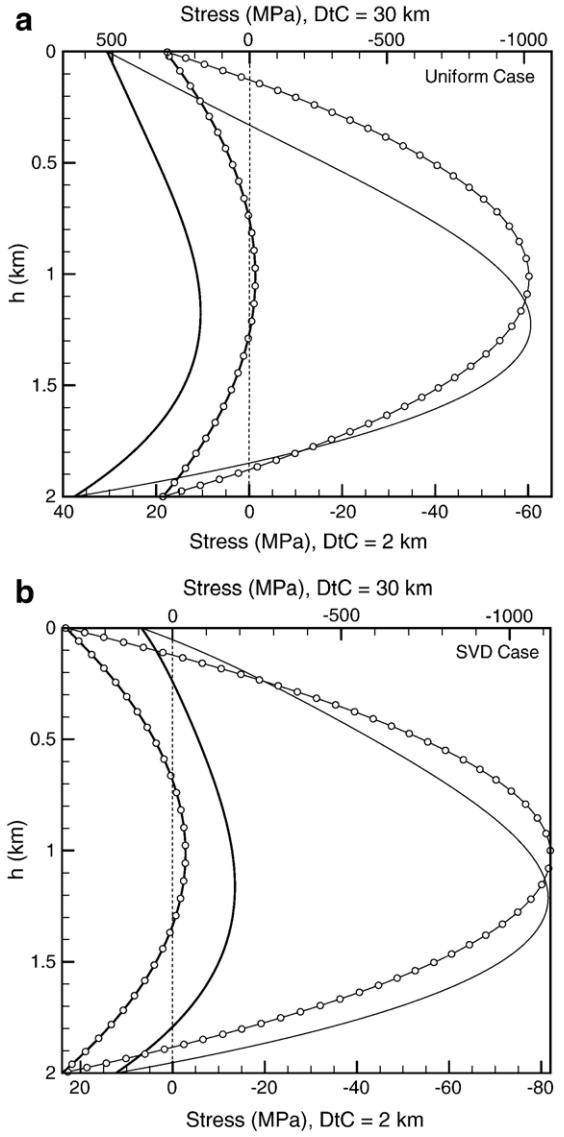

Fig. 8. Failure of a spherical reservoir subjected to uniaxial strain conditions when ρ_m=2600 kg m^{-3}. (a) Uniform host rock density case, $\rho_m=\rho_r$. Tangential stress σ_θ is shown as thick lines, and σ_t is shown as thin lines. The DtC=2 km case is shown as plain lines without markers, the DtC=30 km case is shown as lines with circles. Failure is mathematically favored at the bottom pole, but the difference between the tangential stresses at the top and bottom poles is normally <10 MPa (i.e., on the order of the tensile strength T), suggesting that rupture is almost equally likely at either location. The stresses depicted occur when P=0 MPa. Prior to uniform pressurization a reservoir subjected to uniaxial strain conditions, whether shallow or deep, will fail. Such a reservoir is not physically plausible and would not have been able to form. (b) Smoothly varying host rock density with depth case. Once again, failure occurs even when P=0 MPa. Spherical and ellipsoidal reservoirs are unstable and will not form under elastic conditions when the host rock is subjected to uniaxial strain.

difference between the tensile stresses induced at the two poles of the reservoir is slight, on the order of the 0–10 MPa tensile strength values characteristic of the host rock. With a host density ρ_r=2600 kg m^{-3}, a magma density ρ_m=3400 kg m^{-3} favors failure at the bottom pole by ~10 MPa or less for a 1 km radius reservoir varying in depth-to-center from 2–30 km. For an identical range of depths, if the magma density ρ_m=1000 kg m^{-3} failure at the bottom pole is favored by as little as 1–2 MPa. In cases when the density of the host with depth can be approximated by a single value, as assumed for example by Sartoris et al. (1990) for the Phlegraean Fields in Italy, the magma density and depth of the reservoir have little import to first order, and it appears difficult to promote anything other than vertical intrusion, and potentially surface eruption (which becomes more probable if the magma evolves *in situ* to lower densities), in response to failure of the reservoir walls.

3.2. Sphere, two-layer host rock density

3.2.1. Lithostatic conditions

Uniform density of the host rock is the simplest assumption to make, but it is probably not plausible in many geologic circumstances. The next simplest configuration that has been employed by other researchers is a two-layer density structure for the host material (e.g., Rubin and Pollard, 1987; Parfitt et al., 1993). This model represents what may be considered a simple neutral buoyancy scenario in which the presence of low density rock above higher density rock serves to trap magmas of intermediate density near the neutral buoyancy interface between the two layers. Thus, magma in portions of the reservoir above the interface tends to be denser than the adjacent host rock, while magma below the interface tends to be less dense than its surroundings. The buoyancy forces thus act to pull magma toward the reservoir's mean depth, potentially increasing the chance of failure at this location. To test this hypothesis, magma of density 2600 kg m^{-3} was placed in a reservoir located at the interface between layers of density 2300 kg m^{-3} (upper) and 2900 kg m^{-3} (lower). The results, shown in Fig. 9, illustrate that a two-layer model has only a limited effect on the failure location when compared to the uniform density host configuration. At great depth, the reservoir fails at the upper pole, but as the reservoir approaches the surface the failure location rotates away from the crest, reaching a maximum rotation angle (maximum depth) of $\alpha \approx 58°$. When failure occurs at the crest of the reservoir, σ_t is again equal to σ_θ, and when failure happens away from the crest σ_t is again greater than σ_θ with the result that circumferential intrusion geometries are favored.

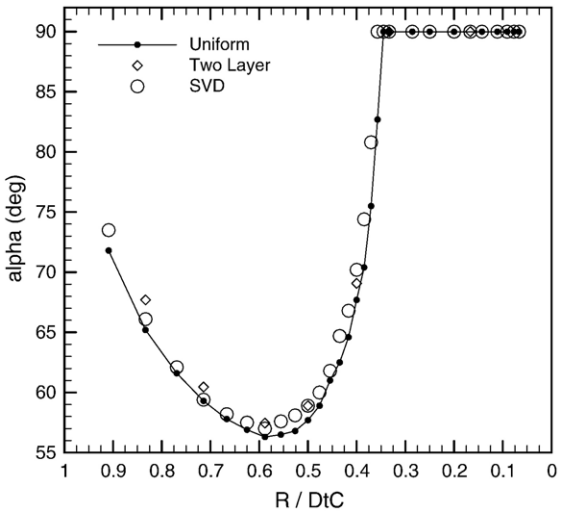

Fig. 9. The location of failure for a spherical reservoir subjected to lithostatic stress is essentially independent of the host rock density structure within which it is located, and σ_t always fails first. For the uniform host rock density model, $\rho_m=\rho_r=2600$ kg m^{-3}. For the two layer model, the interface between the layers always lies at the DtC and $\rho_{ru}=2300$ kg m^{-3}, $\rho_m=2600$ kg m^{-3}, and $\rho_{rl}=2900$ kg m^{-3}. For the smoothly varying density model $\rho_o=2204.4$ kg m^{-3}, $\rho_\infty=2900$ kg m^{-3}, and the magma density is set to the neutrally buoyant value appropriate for the DtC used (see Eq. (18)).

While neutral buoyancy may contribute to cessation of vertical dike ascent and lead to magma stalling, neutral buoyancy conditions do not play a central role in dictating the subsequent failure behavior of reservoirs that form at neutrally buoyant depths.

3.2.2. Uniaxial conditions

Tests of a two-layer model configuration under uniaxial strain conditions again reveals little difference from the uniform density host results discussed previously. All reservoirs examined, centered at depths ranging from 2–30 km, are expected to fail at the poles. On purely mathematical grounds failure is slightly preferred at the bottom pole, but the stress difference between the two locations is again minimal, on the order of at most a few MPa.

3.3. Sphere, smoothly varying host rock density

3.3.1. Lithostatic conditions

Although uniform and two-layer density models may be appropriate in some instances, it is often more physically plausible to expect that the host rock density will vary with depth. In areas where the density structure is controlled by burial and compaction of material emplaced at the surface, Head and Wilson (1992) show that the equation

$$\rho(z)=\frac{\rho_\infty}{1+[(\rho_\infty/\rho_o)-1]e^{\lambda\rho_\infty gz}} \tag{16}$$

adequately describes the density information obtained from seismic wave velocity data for a stack of vesicular basaltic. For their models of volcanic areas on Earth, Head and Wilson (1992) show that a reasonable fit is obtained when the density at great depth (ρ_∞) is taken to be 2900 kg m^{-3}, the density of uncompacted vesicular material at the surface (ρ_o) is 2204.4 kg m^{-3} (this value, a slight modification to the Head and Wilson's best-fit value of 2200 kg m^{-3}, is used for mathematical convenience because it translates neatly to a surface void space fraction of 0.24), and λ is a constant equal to 1.18×10^{-8} Pa^{-1}. Integrating the density from zero to depth z (recalling z is negative at depth) and multiplying by g yields the vertical stress,

$$\sigma_z=-\rho_\infty g\left\{\left[-z+\frac{1}{\lambda\rho_\infty g}\ln\left(1+\left(\frac{\rho_\infty}{\rho_o}-1\right)e^{\lambda\rho_\infty gz}\right)\right]-\left[\frac{1}{\lambda\rho_\infty g}\ln\left(\frac{\rho_\infty}{\rho_o}\right)\right]\right\}. \tag{17}$$

If the depth of reservoir formation is controlled by magma neutral buoyancy relative to the surrounding host, the reservoir depth is a function of the magma density selected, which from Eq. (16) is given by

$$\mathrm{DtC}=-\frac{1}{\lambda\rho_\infty g}\ln\left[\frac{(\rho_\infty/\rho_m)-1}{(\rho_\infty/\rho_o)-1}\right]. \tag{18}$$

To promote ready comparison with the uniform and two-layer density model results reported previously (Fig. 9), the magma density in each smoothly varying host rock density model configuration was set to the neutrally buoyant value at the center of the reservoir; thus a density $\rho_m=2497$ kg m^{-3} is used when DtC=2 km, $\rho_m=2600$ kg m^{-3} when DtC=3 km, etc. Since it has already been demonstrated that the density contrast between the magma and host rock plays little role in controlling the point of failure, not surprisingly the results for the smoothly varying host rock density scenario are quite familiar, with failure occurring at the crest when the reservoir is deeply-seated and rotation away from the crest taking place as the reservoir's proximity to the surface increases (Fig. 9).

3.3.2. Uniaxial strain conditions

The smoothly varying density model configuration under uniaxial strain conditions is qualitatively identical to the previous two uniaxial strain evaluations. All

reservoirs examined will fail at the poles, with failure mathematically favored at the bottom pole by only a few MPa (Fig. 8b).

3.4. Magma pressure, P

Under lithostatic conditions, the minimum uniform magma pressure component P required to initiate tensile failure at any depth for a given reservoir size is essentially independent of gravity and the host rock density structure employed (Fig. 10a). At any specific reservoir depth, however, the pressure required to initiate failure for reservoirs of different radii can be radically different, suggesting that knowing the depth of the reservoir alone is insufficient when selecting an appropriate magma pressure for modeling magma reservoir behavior. Instead, the pressure P required to initiate failure is linearly related ($R^2 > 0.99$) to the ratio R/DtC (Fig. 10b), approaching a limit of three times σ_z for reservoirs formed at very great depth. In addition, for values of R/DtC in excess of ~0.6 (i.e., $\mathrm{DtC} < 5/3R$), the pressure required to initiate failure is, on purely mathematical grounds, less than the magnitude of the vertical stress at the reservoir's center. This issue is examined in Section 4.6 in greater detail.

Under uniaxial strain conditions, tensile failure occurs at the poles of the reservoir even when the uniform magma pressure $P=0$, i.e. the spherical cavity will fail when loaded by the weight of the enclosed magma alone, no other pressure component is required (Fig. 8). At large depths, in fact, the majority of the reservoir wall exists in a state of tension, a situation which is clearly implausible on physical grounds. The percentage of the wall subjected to tensile stress and hence failure when $P=0$ decreases as the depth of the reservoir decreases, but even when the reservoir is quite shallow a significant portion of the wall is unstable. For instance, when $R=1$ km and $\mathrm{DtC}=30$ km, Fig. 8a demonstrates that a state of tension exists at the crest of the reservoir, if $T=10$ MPa, for roughly $h \leq 700$ m, or $\alpha \geq 17°$, and a similar failure zone exists at the bottom pole of the reservoir; likewise, if $\mathrm{DtC}=2$ km, the vast majority of the wall is unstable. The implications for the instability of shallow reservoirs under uniaxial strain conditions were explored previously by Sartoris et al. (1990), and are discussed further in Section 4.7.

3.5. Non-spherical ellipsoidal reservoirs

In general terms, the time-averaged three-dimensional geometry of many magma reservoirs is well approximated by ellipsoids (Fedotov, 1982), a geometrical class within which spheres represent only a special case. As their eccentricities deviate from the spherical, axisymmetric

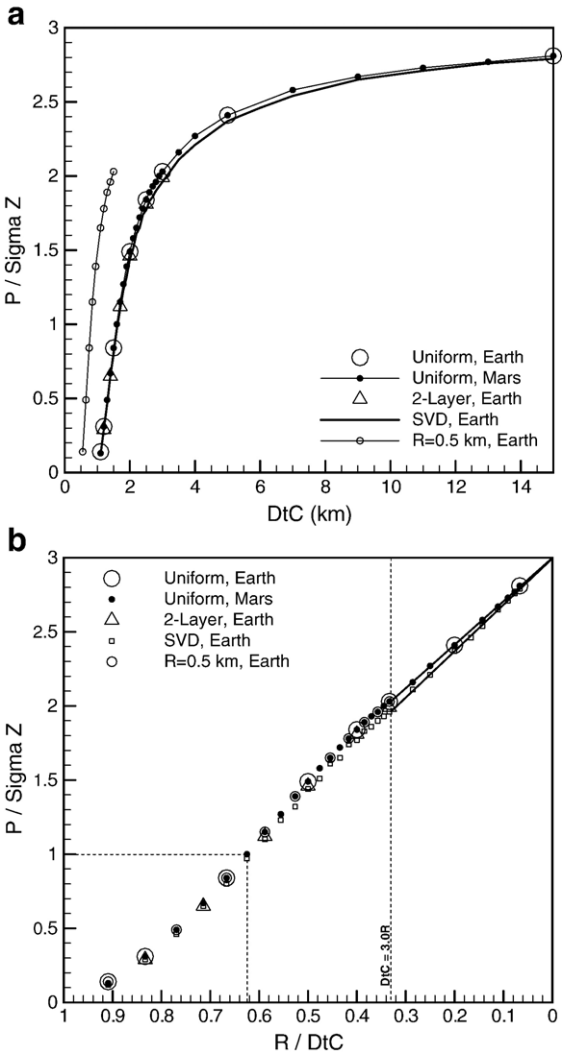

Fig. 10. Uniform pressure P required to induce initial failure, expressed as a multiple of the host rock vertical stress σ_z at the reservoir DtC. (a) When $R=1$ km, the pressure P required to cause rupture for any given DtC is effectively independent of the host rock density structure and non-zero value of gravity selected. The value of P required is not, however, independent of R, as shown for a uniform density model when $R=0.5$ km. Self-consistent treatment of reservoir pressures requires knowledge of both the depth of a reservoir as well as its size; simply setting $P=\sigma_z$ at the DtC or crest, as is done in some modeling efforts, is insufficient to characterize reservoir pressures in an elastic model. (b) When P is plotted against R/DtC, it becomes evident that there is a near-linear relationship between the two, independent of the value selected for R, the host rock density structure, or gravity. When $\mathrm{DtC} \geq 3R$ the linear fit yields $R^2=0.999$, and as $R/\mathrm{DtC} \rightarrow 0$ then $P \rightarrow 3\sigma_z$ for failure to occur. At $\mathrm{DtC} < 3R$ the linear trend varies slightly due to the proximity of the free surface, but a fit to the full dataset still yields $R^2=0.99$. When $P < \sigma_z$ failure would occur before the reservoir could become stable. Thus, reservoirs within an elastic host subjected to lithostatic stress are unstable when $\mathrm{DtC} \approx 1.6R$ or less.

ellipsoids are expected to concentrate greater amounts of stress in the vicinity of the reservoir wall where it intersects the major axis, potentially serving to enhance failure near this location. While a wide array of ellipsoidal geometries are possible, investigation here is limited to a few representative axisymmetric configurations to elucidate the differences in behavior between these geometries and spherical reservoir model results.

3.5.1. Prolate ellipsoids

For a prolate ellipsoid with vertical major axis $a=1.25$ km and horizontal minor axis $b=0.894$ km (volume identical to a spherical reservoir with $R=1$ km), stress will be concentrated near the poles of the reservoir and failure is enhanced at these locations. The failure angle α is given for a prolate reservoir by

$$\alpha = 90 - \tan^{-1}\left\{\frac{b\left[1-\left(\frac{a-h}{a}\right)^2\right]^{0.5}}{a-h}\right\}. \quad (19)$$

The surface effect seen with a sphere, which rotates the point of failure away from the top pole of the reservoir under lithostatic conditions, occurs as well with prolate ellipsoids, but the effect is inhibited and the failure location remains much closer to the upper pole (Fig. 11), promoting in effect only vertical dike emplacement. This result is insensitive to the host rock density structure employed, to gravity, and to plausible magma density variations.

Under uniaxial strain conditions stress enhancement due to the prolate geometry is once again sufficient to induce failure in most instances even when the only stresses applied to the interior wall of the reservoir stem from the weight of the enclosed magma. These stresses are greatest at the bottom of the reservoir, and it is at this location that failure occurs.

3.5.2. Oblate ellipsoids

For an oblate ellipsoid with horizontal major axis $a=1.25$ km and vertical minor axis $b=0.64$ km (volume again identical to a spherical reservoir with $R=1$ km), the failure angle is defined by

$$\alpha = 90 - \tan^{-1}\left\{\frac{a\left[1-\left(\frac{b-h}{b}\right)^2\right]^{0.5}}{b-h}\right\}. \quad (20)$$

For this oblate geometry, failure typically occurs under lithostatic conditions within a few degrees of the midpoint of the reservoir except when the reservoir is located at very shallow depth (Fig. 11). The tangential stress σ_t greatly exceeds the circumferential stress σ_θ, and hence lateral sill injection will be the favored intrusion geometry when the reservoir wall fails near the midpoint. The pressure P required to initiate failure at any given DtC is less than that of the spherical geometry when the reservoir is deep-seated, reflecting the enhanced stress concentration that results from the oblate geometry; however, at shallow depths, where the proximity of the surface plays a role, the pressure P required for oblate reservoir failure to occur tends to slightly exceed that required for the sphere because the top of the oblate reservoir is further from the surface than the top of a sphere with comparable volume at the same depth.

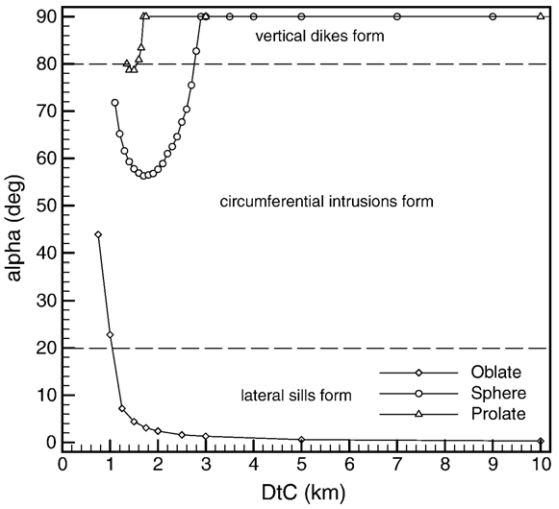

Fig. 11. Effect of geometry on failure location; rough qualitative division of the plot into zones denoting the favored style of intrusion inferred is performed to summarize the quantitative results. Adoption of a mildly prolate ellipsoidal geometry yields a failure pattern similar to that of a sphere with the same volume, but because the geometry concentrates even more stress at the upper and lower poles the rotation away from the crest at shallow depths is more difficult to achieve, and the net magnitude of the rotation induced is damped out. Failure will almost always favor vertical dike injection. For a mildly oblate ellipsoidal geometry of identical volume, however, the failure pattern is quite different, as the stress concentration induced by the geometry drives failure toward the reservoir DtC. In this case, as with the spherical and prolate examples, σ_t continues to fail first. Thus failure of an oblate reservoir will favor lateral sill injection, but not injection of lateral dikes.

Under uniaxial strain conditions the geometric factors driving oblate geometries to fail near the middle of the reservoir compete with the tendency for failure to occur near the poles due to the host rock stress state. For the reservoir geometry examined, the host rock stress state dominates and failure occurs at the poles; however, while the effect is not quantified here, as the reservoir eccentricity increases (i.e., the reservoir becomes more sill-

like) the stress concentration due to the oblate geometry is expected to overcome the host rock stress and move the failure location back toward the midpoint of the reservoir. In the instance modeled, failure is mathematically favored at the upper pole at all depths examined (DtC from 1.5–10 km), but once again the difference between the tensile stresses at the two poles is minimal (~1 MPa), suggesting that failure could occur readily at either location.

3.6. Summary of results

The preceding analysis demonstrates that failure at or near the crest (lithostatic cases) or poles (uniaxial strain cases) of a spherical magma reservoir is achieved readily under a wide variety of physical circumstances. Failure near the midpoint of a spherical reservoir (i.e., $\alpha \approx 0°$) is not predicted under any of the geological parameter configurations explored. For a host rock characterized by lithostatic stress, under the purely elastic conditions explored here the uniform pressure P required to initiate failure of the reservoir walls is a linear function of the ratio R/DtC, and as $R/\mathrm{DtC} \rightarrow 0$ the maximum uniform pressure $P \rightarrow 3\sigma_z$ where σ_z is the undisturbed vertical host rock stress at DtC, the reservoir's midpoint depth. Failure occurs at the crest of the reservoir ($\alpha = 90°$) for $\mathrm{DtC} > 3R$. At shallower depths than this the proximity of the free surface affects the failure location in a fashion that promotes circumferential intrusion, with a maximum rotation from the crest (i.e., maximum depth of failure within the reservoir) of $\alpha \approx 56°$ occurring when $\mathrm{DtC} \approx (5/3)R$. In contrast to the lithostatic case, when the host rock is characterized by uniaxial strain failure of the reservoir walls occurs at the poles, with failure usually mathematically favored to a slight degree at the bottom pole. Failure is typically predicted, however, even when the uniform pressure $P = 0$. This implies that a pressurized spherical reservoir is unlikely to form or be stable under uniaxial strain conditions.

The geometry of a prolate ellipsoidal reservoir simply enhances what is observed in the spherical case. Failure occurs at or very near the poles for every geological and geometrical configuration examined. A "surface effect" like that seen for the spherical geometry is observed under lithostatic conditions but the effect is severely inhibited. Under uniaxial strain conditions, like in the spherical geometry case, failure is again predicted to occur at either pole with similar ease.

In contrast, under lithostatic conditions the geometry of an oblate ellipsoidal reservoir promotes failure near the midpoint, and favors lateral sill injection, unless the reservoir is located at very shallow depth; this is the only combination of geometrical and geological parameters examined which promotes classical lateral intrusion of any kind. Under uniaxial strain conditions, the oblate geometry examined once again fails at both poles with almost equal ease, demonstrating the degree of control exerted by the host rock stress state over the failure location. While not explicitly quantified here, however, when oblate reservoirs are thinner and hence more sill-like, enhancement of stress at the increasingly crack-like reservoir midpoint should eventually return failure to this location even under uniaxial strain conditions.

4. Discussion

Using analytical and numerical approaches, many authors have examined spherical magma reservoirs within an elastic host rock subjected to lithostatic stress in an effort to understand the circumstances leading to, and the characteristics of, their failure in response to overpressurization. Published model results can differ considerably, however, even when common suites of geometrical and geological factors are treated.

4.1. Sphere in an infinite host lacking depth-dependent stresses

One common approach used in analytical models is laid out by several authors (e.g. Gudmundsson, 2002). Procedurally, the reservoir is defined as a thick-walled spherical cavity, of inner radius R and outer radius R_2, with $R_2 \gg R$ to eliminate surface effects. The shell is subjected only to a uniform internal fluid pressure P and a uniform external stress P_l. The excess pressure within the reservoir P_e is defined as

$$P_e = P - P_l \tag{21}$$

and the radial stress in spherical polar coordinates becomes

$$\sigma_r = P_e \left(\frac{R}{r}\right)^3 \tag{22}$$

where r in this case is the radius vector extending out from the center of the sphere. This equation is equivalent to that given by Eq. (10), and similar derivation for the induced tangential stresses yields a relationship identical to that described by Eq. (11).

Models formulated in this fashion reduce the reservoir to a pressurized sphere in an infinite medium, and suffer from three fundamental problems when they are used to examine failure and related phenomena such

as the pressure that a reservoir can sustain. First, the mathematics used to derive the relationship between the normal stress balance across the reservoir wall and the induced stress parallel to the wall (e.g., Timoshenko and Goodier, 1951) require an absence of depth-dependent stresses, i.e. the normal stress balance across the reservoir wall must be constant with depth. Even in the simplest of models, this condition can normally only be achieved when the magma and host rock densities are equal and depth-invariant. Second, such models fail to incorporate the compressive, wall-parallel component of the host rock stress, an important depth-dependent factor which also resists the rupture process. Third, because the model formulation fails to introduce (and correct for) displacement and stress variations caused by the presence of the free surface, in effect only deep-seated reservoirs can be analyzed. Given these three restrictions, it is evident that this type of analytical model should be used with great caution when exploring magma reservoir failure under normal geological circumstances.

4.2. Half-space models: effect of the free surface

Since many magma reservoirs form close to the surface, it has long been recognized (e.g., Jeffery, 1921) that the presence of the surface will modify the stress distribution around the walls of the cavity and hence will affect calculations exploring where and how the walls will fail in response to overpressurization. While the free surface effect is ignored in some recent analytical studies (e.g., Tait et al., 1989; Gudmundsson, 2002), efforts to correct for the free surface effect have been introduced into many others (e.g., McTigue, 1987; Gudmundsson, 1988; Bonafede, 1990; Parfitt et al., 1993; Pinel and Jaupart, 2003; Pinel and Jaupart, 2004). In essence, these models adopt a correction factor, here called C (following Parfitt et al., 1993), which is given in simplest form by Jeffery (1921), who derives it for an infinite horizontal cylinder in the absence of other depth-dependent stresses as

$$C = 1 + 2\tan^{-1}\phi \tag{23}$$

where ϕ is the angle between the vertical axis passing through the center of the cylinder and a line connecting the point of intersection between the rotation axis and free surface with any point on the reservoir wall (i.e., for a reservoir at reasonable depth $\phi = 0$ at the upper and lower poles and reaches a maximum value at the midpoint of the reservoir, where $\alpha = 0$). Tensile failure will occur where the line connecting the point of intersection between the rotation axis and free surface with the reservoir is tangent to the wall. McTigue (1987) independently derives an approximate correction describing the free surface effect for a pressurized sphere in a half space lacking other depth-dependent stresses. He demonstrates that the location of failure predicted is nearly identical to that of Jeffery (1921), and thus that the failure location is also well described by the point of tangency, given by

$$\alpha = 90 - \cos^{-1}(R/\mathrm{DtC}). \tag{24}$$

If the magma body is treated as an internally pressurized vessel which is not subjected to depth-dependent stresses—a condition achieved only if wall-parallel host rock lithostatic stress components are ignored and if the magma and host rock densities are set equal to one another and invariant with depth—Fig. 12 shows the effect the free surface will have upon the location of failure according to the analytical corrections. Not surprisingly given their common origin, the analytical model results are in strong agreement with one another. If gravity is turned off in the numerical model, reducing the FEM formulation in similar fashion to a pressurized sphere in a half space (i.e., this zeroes out all host rock and magma loading components except for the internal uniform pressure P), the failure locations predicted by the finite element model align closely with the locations predicted by the analytical models. This agreement establishes that published analytical correction factors account accurately for the effects of the free surface when depth-dependent stresses are eliminated, and that the current FEM can account for the free surface effect with a comparable degree of precision. In addition, however, Fig. 12 indicates that the differences between the depth-invariant half-space model predictions and those of the full FEM, where depth-dependent gravitational factors are re-introduced, are not caused by an inability of the FEM to account for free surface effects.

4.3. Sphere in a half-space with depth-dependent stresses

Analytical efforts to augment 'sphere in an infinite medium' models with depth-dependent stresses–including wall-parallel host rock stresses and free surface effects–have been made, most notably by Parfitt et al. (1993) in their detailed treatment of failure for spherical magma reservoirs under lithostatic conditions. Several challenges face this approach, however, and because the outcome is sharply different from the numerical model results (Fig. 12) it becomes necessary to explore the causes in detail.

4.3.1. Summary of published analytical model

Parfitt et al. (1993) base their analysis on two key equations, assessed below using only the simplest and most internally self-consistent case, i.e. one in which the magma and host rock densities are uniform and equal to one another to minimize depth-dependent normal stresses across the reservoir wall. First, preserving their notation,

$$P_t(h) = P_{\mathrm{m}}(h) + P_B \tag{25}$$

where $P_t(h)$ is the total pressure in the magma at a depth h below the reservoir roof, P_B is the excess pressure which has accumulated in the magma due to repeated injections (and acts uniformly over the reservoir walls), and $P_{\mathrm{m}}(h)$ is the pressure at any depth due to the weight of the overlying magma. Second, Parfitt et al. assume that failure will occur when the tangential stress exceeds the tensile strength of the rock, and thus (see Eq. (11)) when the normal stress balance across the wall of the reservoir exceeds twice the tensile strength of the rock (Tait et al., 1989), so that

$$P_t - P_{\mathrm{L}} = 2T \tag{26}$$

where P_{L} is the lithostatic stress in the host (i.e., $\rho_r gz = \rho_r g(D_T + h)$, where z (positive in the analytical models) is depth below the surface and D_T is the depth to the reservoir crest), and T is the tensile strength of the rock (in this instance replacing their notation, σ_T, to avoid confusion with the tangential stress). Following Gudmundsson (1988), who shows that Eq. (11) must be modified for the half-space case by multiplying the normal stress balance by C, the final failure equation becomes

$$P_t - P_{\mathrm{L}} = 2T/C. \tag{27}$$

Even though the source stress is depth-dependent (which was not the case when C was derived), Parfitt et al. state that it gives the trend of the effects of the free surface adequately for their purposes. Eqs. (25) and (27) are then combined to yield the equation for calculating the excess pressure required to cause failure at any given depth h, which is

$$P_B = (2T/C) + P_{\mathrm{L}} - P_{\mathrm{m}}. \tag{28}$$

In the simplest case analyzed here, with the magma and host rock densities uniform and equal, this reduces to

$$\begin{aligned} P_B &= (2T/C) + \rho_r g(D_T + h) - \rho_m gh \\ &= (2T/C) + \rho_r g D_T. \end{aligned} \tag{29}$$

It is worth noting that Parfitt et al. mistranslate the correction factor employed, defined by Eq. (23), into

$$C = \frac{[2h(R + D_T) + D_T^2]}{(h + D_T)^2}. \tag{30}$$

The correct equation for C is

$$C = \frac{[2h(2R + D_T) + D_T^2 - h^2]}{(h + D_T)^2}. \tag{31}$$

While the difference between Eqs. (30 and (31) affects the magnitude of C and hence the pressure P_B required to induce failure, it does not change the failure location predicted, and thus the locations reported by Parfitt et al. (1993) are not affected.

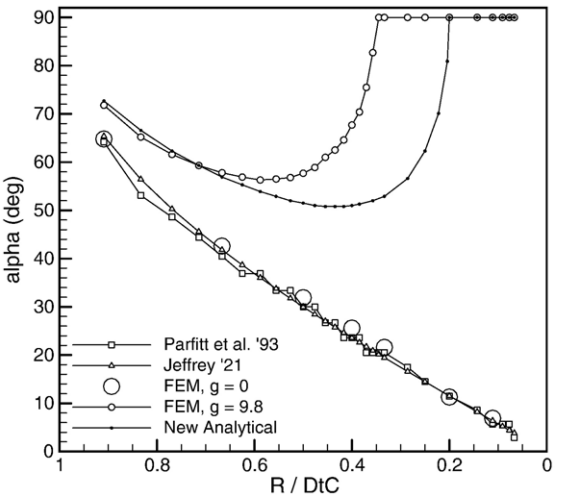

Fig. 12. Comparison between the failure location behavior predicted by the current study and what is predicted by analytical models which correct for the free surface. To promote direct comparison, a uniform density host rock subjected to lithostatic conditions is employed; T=0 MPa, and either g=0 m s^{-2} or $\rho_{\mathrm{m}} = \rho_r$ and g=9.8 m s^{-2}. The solutions shown for Parfitt et al. (1993) and Jeffery (1921) are representative of and essentially identical to those of others (e.g., McTigue, 1987; Gudmundsson, 1988), and having reduced the reservoir to an internally pressurized sphere in a half space (g=0 m s^{-2} condition) they predict failure rotating from a location near the top of the reservoir toward the mid-depth as reservoirs form at increasing depths. The same behavior is predicted using the FEM when depth-dependent stresses (other than those induced explicitly by the free surface) are eliminated by setting g=0 m s^{-2}, once again reducing the model to a pressurized sphere in a half space. In the gravitationally loaded configuration, with magma and host rock densities set equal, the failure location predicted by Parfitt et al. remains unchanged, but a reformulated analytical model (New Analytical) that includes wall-parallel lithostatic stress components and a modified failure criterion yields failure behavior that is both consistent with simple thought experiment predictions (cf. Section 3.1.1) and analogous to the FEM model results; see Section 4.3 for detailed discussion.

Comparison between results obtained using this system of equations by Parfitt et al. (1993) and the numerical modeling results obtained here (Figs. 10 and 12) indicates significant disagreement. These differences are assessed below by re-deriving the analytical model from first principles and then comparing the predictions from both analytical models with the numerical model results, focusing specifically upon (a) the excess pressure required to cause rupture, and (b) the rupture location.

4.3.2. Reformulated analytical model

Going back to first principles, the magma pressure at any given depth h within a reservoir can be expressed, using Eq. (4), as

$$P_t = P + P_{\mathrm{m}} = (\rho_r g D_T + k) + \rho_m g h. \tag{32}$$

A logical way to express the uniform pressure component is as the sum of the minimum value for P required to prevent collapse, i.e. the lithostatic stress value at the top of the reservoir, and any additional uniform pressure k that can be derived through infusion of magma or other physical mechanisms. Note that this is not equivalent to the Eq. (25) starting point assumed in Parfitt et al.'s (1993) formulation unless P_B is defined as the sum of the pressure at the top of the reservoir plus an additional uniform component. This seems unreasonable for two reasons: (1) P_B, labeled as an excess pressure, would normally be more akin to k alone by definition; and, (2) characterizing P_B as the sum of these two components is inconsistent with what is required for quantitative reproduction of the data presented in Parfitt et al.'s figures.

The normal stress balance across the wall is defined as the difference between the magma pressure at some depth h and the host rock lithostatic stress perpendicular to the wall at the same depth, thus

$$\begin{aligned} P_t - P_{\mathrm{L}} &= P + P_{\mathrm{m}} - P_{\mathrm{L}} = (\rho_r g D_T + k) + \rho_m g h \\ &\quad - (\rho_r g D_T + \rho_r g h) \end{aligned}$$

$$\text{i.e., } P_t - P_{\mathrm{L}} = k + (\rho_m - \rho_r) g h. \tag{33}$$

Proceeding with the derivation, recall that Gudmundsson (1988) shows that modification by the free surface requires that

$$\begin{aligned} \sigma_t &= |[-(P_t - P_{\mathrm{L}})/2](1 + 2\tan^2\phi)| \\ &= [(P_t - P_{\mathrm{L}})/2]C. \end{aligned} \tag{34}$$

Outward expansion of the reservoir, driven by the normal stress balance across the wall, will result in rupture once the magnitude of the tensile stress being generated exceeds the sum of the factors resisting rupture, i.e. the tensile strength plus the wall-parallel component of the lithostatic stress. Thus, failure occurs at any given depth when

$$\sigma_t = T + P_{\mathrm{L}} = T + \rho_r g (D_T + h). \tag{35}$$

Combining Eqs. (33), (34) and (35) then yields, at failure,

$$[k + (\rho_m - \rho_r) g h](C/2) = T + \rho_r g (D_T + h). \tag{36}$$

Solving for k, the additional uniform pressure required to induce rupture is

$$k = \frac{2T}{C} + \frac{2\rho_r g D_T}{C} + \rho_r g h \left(\frac{2}{C} + 1\right) - \rho_m g h \tag{37}$$

or, if the magma and host rock densities are set equal to one another, then

$$k = \frac{2T}{C} + \frac{2\rho_r g (D_T + h)}{C}. \tag{38}$$

4.3.3. Comparison of analytical models and FEM results

Inclusion of both the free surface and depth-dependent variations in the normal stress balance across the reservoir wall in analytical models, as laid out by Parfitt et al. (1993) and in the reformulated model above, seeks to make them better representations of the physical conditions that characterize magma reservoirs. This improvement over models that depict the reservoir as a uniformly pressurized sphere in an infinite medium, however, comes at a price. The approaches employed to develop the analytical models suffer from a common flaw in that they must mix depth-independent conditions and mathematical derivations (the normal-to-tensile stress relationship of Eq. (11); derivation of the free surface correction factor C as laid out by Jeffery (1921), McTigue (1987), etc.) with additional depth-dependent stress conditions (e.g., variation in lithostatic and magma weight terms with depth) that directly violate the depth-independent assumptions. These kinds of analytical model formulations are thus not ideally suited to the problem being explored, and the question is one of how significant the introduced errors become. In contrast, a numerical finite element model that can incorporate all the boundary stresses and body loads explicitly, without requiring simplifying assumptions about the outcome of their interactions, is well suited to such explorations. The simplest analytical conditions—which reduce the problem to a uniformly pressurized sphere in a half space—serve as an excellent way to

calibrate the FEM. Thereafter, however, the FEM becomes the benchmark against which the success of more complicated analytical models can be tested.

Fig. 12 demonstrates that the Parfitt et al. (1993) analytical formulation and the FEM yield equivalent results under identical, depth-independent conditions equivalent to a uniformly pressurized sphere in a half space. The Parfitt et al. formulation is reduced to this condition by setting gravity equal to zero, which eliminates all depth-dependent stresses from the problem. The result, examining Eq. (28), shows that the minimum excess pressure P_B required to induce failure is solely dependent upon the magnitude of C, and will occur where C is greatest. Eq. (30) or (31) demonstrates that this location depends upon the depth h within the reservoir, and thus the location of failure and pressure required are uniquely constrained. The reformulated analytical model, Eq. (37), yields identical results with gravity set to zero. Within the FEM, setting gravity equal to zero also eliminates all stresses except for the uniform component P of the magma pressure, and the failure depth and pressure required are equally well constrained. Under these conditions, all three models show that failure of deep-seated magma chambers is favored near the reservoir's mid-depth, while shallower reservoirs fail at shallower depths (larger α).

Returning to gravitationally-loaded conditions, which for the analytical model means that they will incorporate the problems discussed earlier, the most useful comparison involves setting the magma and host rock densities equal to one another, so that the rate-of-change of the load normal to the reservoir walls is balanced, eliminating this otherwise depth-dependent component of the problem. For the Parfitt et al. (1993) model, examination of Eq. (29) shows that while the magnitude of P_B required to induce rupture will change, the location of failure will not as all factors other than C are constant, i.e. independent of depth h within the reservoir. The failure location (with $T=0$ MPa) shown in Fig. 12 is thus unaltered; the pressure required to induce failure when $T=10$ MPa is reported in Table 1.

In contrast, the failure location predicted using the FEM alters substantially when the model is gravitationally loaded (Fig. 12). As discussed previously, failure is predicted to occur at the crest of the reservoir until the reservoir DtC becomes so shallow that free surface effects rotate the failure location to greater depth h within the chamber. The correctness of this behavior, at least for the deep-seated case, is quickly established through comparison with the simple thought experiment laid out in Section 3.1.1 (and Fig. 5). Why then do the Parfitt et al. (1993) model results differ?

Table 1
Uniform pressure required to cause failure

DtC (km)	Parfitt (MPa)	New Model (MPa)	FEM (MPa)
1.5	45.1	35.3	43.6
2.0	78.7	79.1	92.8
3.0	136.7	165.8	175.8
4.0	190.7	247.4	250.7
5.0	243.4	325.7	327.4
7.0	347.2	478.6	479.8
9.0	450.1	631.5	632.9

Comparison of failure characteristics predicted by analytical and numerical models when $R=1$ km, $\rho_r=\rho_m$, and $T=10$ MPa. The Parfitt et al. (1993) pressure is the uniform pressure obtained when the minimum P_B for a given reservoir configuration, calculated using Eq. (29), is added to the lithostatic stress at the depth where failure is predicted to occur, consistent with their formulation. The New Model pressure is calculated by adding the minimum k from Eq. (38) to the lithostatic stress at the crest of the reservoir, consistent with this model's formulation. The FEM pressure is obtained from the current numerical modeling effort (adjusted for the difference in T, as in Fig. 6).

The answer becomes clearer through comparison of the differences between the reformulated model and that of Parfitt et al. (1993). The first difference is the introduction into the reformulated model of an important depth-dependent term (Eq. (35)) that is not included by Parfitt et al.: the wall-parallel component of the host rock lithostatic stress. With the introduction of this component, which will be present in a natural system and which is also explicitly included (and tested for) in the FEM, rupture can only occur at any given depth once the wall-parallel extension induced by the normal stress balance across the reservoir wall exceeds the sum of the tensile strength and the wall-parallel lithostatic stress. The second difference is that re-derivation of the normal stress balance from first principles shows that, for Eq. (25) to be correct, the excess pressure P_B term used by Parfitt et al. has to equal the lithostatic stress at the crest of the reservoir plus some constant value. This is not consistent with the definition of excess pressure, typically defined as the magma pressure above lithostatic, suggesting that their total magma pressure P_t is calculated incorrectly. When these two differences are taken into account, the characteristics of the reformulated analytical model begin to resemble the FEM predictions (see Fig. 12 and Table 1). Specifically, Fig. 12 shows that the reformulated model predicts failure at the crest when the reservoir is deeply-seated, with failure rotating away from the crest and then back toward it again for reservoirs formed at increasingly shallow depths. Similarly, Table 1 shows that the pressures required for failure in the reformulated analytical model and FEM are quite similar. While differences between the reformulated analytical model and FEM are obvious,

these occur principally when the reservoir is located at shallower depths; the key difference is that the reformulated model begins to 'feel' the presence of the free surface too early, when DtC=5R (for the FEM it is DtC=3R). The error stems (as discussed earlier) largely from the mixture of depth-independent derivations (i.e., for C and in Eq. (11)) with depth-dependent factors in the analytical formulations, and increases in importance as C gets larger and as the increasing proximity of the surface leads to increasing asymmetry of the reservoir wall displacements (see Section 4.4). It is unreasonable to expect that the reformulated analytical model, for the reasons cited above, will exactly match the characteristics of the FEM except in the simplest of situations. However, in spite of the fact that the new analytical model has ample room for improvement, its general characteristics (failure at the crest at large DtC; rotation of the failure location away from the crest at small DtC; maximum rotation to $\alpha \approx 55°$; pressure magnitudes required for failure) demonstrate quite clearly that incorporation of important stresses missing from the Parfitt et al. (1993) model goes a long way toward explaining why the predictions of the latter and the predictions of the FEM differ so strongly.

4.4. Failure location and orientation and resulting intrusion style

When failure occurs near the crest of the reservoir, regardless of whether it is σ_t or σ_θ that induces first failure, the result will be a vertical dike if magma intrudes into the host rock. As the point of failure rotates away from the crest, however, it becomes important to constrain which wall-parallel stress causes failure to occur if insight into intrusion geometry is desired. For instance, if the failure location is at $\alpha=60°$ then radial dikes will initiate if σ_θ first exceeds the tensile stress, whereas circumferential geometries will be favored if σ_t instead overcomes the tensile stress to induce initial failure. Similarly, if failure occurs near $\alpha=0°$ then either lateral sills ($\sigma_t > \sigma_\theta$) or dikes ($\sigma_\theta > \sigma_t$) could in theory form. Since separate calculation of σ_θ and σ_t is seldom possible in analytical models, which are commonly framed by assuming conditions for which σ_θ and σ_t must be identical, knowledge of resultant intrusion geometries should not be claimed with any confidence using such results. For all numerical models run here, failure at locations away from the crest (Fig. 12) always occurs in the σ_t orientation, i.e. one which favors the formation of circumferential (ring- or cone-like) features or lateral sills.

The failure location is dictated by the deformation of the reservoir wall, which becomes increasingly asymmetric at shallow depths due to the presence of the free surface. For a reservoir with $R=1$ km and DtC=2 km (uniform density model, lithostatic conditions), Fig. 13a and b compare the radial and vertical components of displacement at the reservoir wall in a gravitationally loaded half space with the displacements predicted analytically (Timoshenko and Goodier, 1951). The radial component is nearly unaffected by the presence of the free surface, whereas the vertical component undershoots the analytical displacements across the bottom of the reservoir and increasingly overshoots it toward the crest. Fig. 13c shows the net displacement of the reservoir wall based on the analytical and numerical calculations (both exaggerated by a factor of 1500 for visibility). For this reservoir geometry, the approximate failure location expected is denoted by the grey-shaded region, with $\alpha \approx 57°$. Exploration using the numerical model results for several different DtC values (from 1.4 km to 5 km) reveals that rupture occurs in the area of the reservoir wall where the strain deviation in the σ_t-direction is greatest; the difference in the h predicted for the failure location using σ_t (Fig. 9) and the depth h at which the maximum strain deviation occurs is on the order of 50 m or less. Since the conditions at the wall of the reservoir require that σ_t, σ_θ and σ_r are principal stresses, the strain in the σ_t-direction (ε_t) is determined from standard stress–strain equations for an isotropic, three-dimensional, linearly-elastic solid, and the strain deviation at any location along the wall is then simply the strain ε_t minus e, the mean normal strain (Jaeger and Cook, 1979).

It is worth noting explicitly that the current finite element treatment is only used here to predict what the favored intrusion geometry will be near the reservoir, operating under the assumption when doing so that the geometry will be governed by the location and alignment of the tensile failure predicted. Further from the reservoir, the fate of the intrusion will of course be governed by the rheology of the magma, the driving pressure, the host rock stress state, stresses resulting from the intrusion itself, and many other temporally- and spatially variable factors discussed extensively in the literature (e.g., Anderson, 1936, 1951; Rubin and Pollard, 1987; Lister and Kerr, 1991; Parfitt and Head, 1993; Rubin, 1995b).

4.5. Vertical displacement at the surface

Most analytical and numerical models of magma reservoir failure are designed to explore displacements at the free surface. The spatial distribution of surface displacements arising from a subsurface event, in this

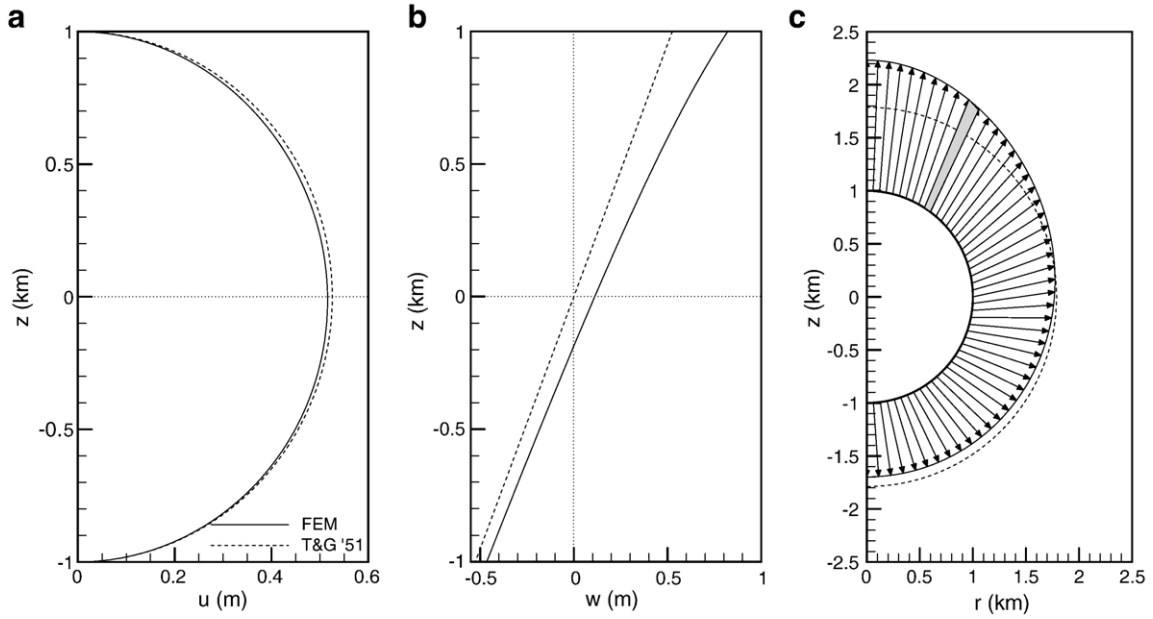

Fig. 13. Analytical versus numerical displacements, $R=1$ km, DtC=2 km, uniform density configuration; $z=0$ km defines the reservoir center. (a) Displacement in the radial direction as a function of depth varies only minimally. Analytical prediction (Timoshenko and Goodier, 1951), using Eq. (8), is based on a uniform pressure P of 50.45 MPa, the difference between the lithostatic pressure at the crest of the reservoir (25.48 MPa) and the pressure required to induce rupture (see Section 4.5). The uniform pressure P for the gravitationally loaded FEM is that required to induce rupture, 75.93 MPa (see Fig. 10b). (b) Displacement in the vertical direction. The numerical model predicts less displacement than the analytical calculation (Eq. (9)) in the lower half of the reservoir, but significantly more displacement in the upper half of the reservoir due to the proximity of the free surface. (c) Total displacement of the reservoir wall, exaggerated by a factor of 1500 to enhance the visibility of the pattern. The proximity of the free surface enhances the asymmetry of the displacement pattern. The predicted rupture location (in this model and others tested) is coincident with the area where the maximum strain deviation in the σ_r-direction occurs (grey-shaded box).

case pressurization of a magma reservoir, is a quantity that can be measured in the field, and because of the potential hazards posed by active magma systems it is desirable to extract as much information about the subsurface activity from surface measurements as possible. There is thus an extensive body of literature dedicated to this topic, and while the focus of the current paper is upon gaining insight into failure of the reservoir walls, comparing the current FEM results with existing displacement solutions yields insight into both. Discussion is limited here to models in which the host rock and magma densities are equal and invariant with depth.

As an initial comparison, Fig. 14a plots the two most commonly employed analytical solutions for the vertical displacement (Mogi, 1958; McTigue, 1987) as a function of r, the radial distance from the axisymmetry axis, assuming $R=1$ km, DtC=5 km, $P=10$ MPa, $\nu=0.25$ and $G=24$ GPa; this geometry is explicitly chosen to reduce free surface effects. The analytical uplift predictions are then compared with three different sets of results from the current study. First, after setting $g=0$ in order to reduce the numerical model to a uniformly pressurized sphere in an infinite half space, the same condition modeled by both Mogi (1958) and McTigue (1987) analytically, the solution shown is a reasonable match but predicts roughly 0.25 mm less surface displacement than the McTigue (1987) model. Fitting the analytical data more closely (for $r/\mathrm{DtC}<\sim 2$) requires increasing the reservoir pressure by ~0.15 MPa in the FEM or decreasing the reservoir depth by ~50 m, indicating that the difference between the two model approaches is on the order of 1–2%. If gravity is incorporated back into the FEM, a situation reflecting the circumstances of a real reservoir, the usefulness of the gravity-free solution is validated. To match McTigue's (1987) displacement solution at $r=0$ (and to yield a good fit for $r/\mathrm{DtC}<\sim 2$) requires a pressure $P=112.1$ MPa. This is, however, simply the lithostatic pressure at the crest of the reservoir (~102 MPa) plus the stated excess pressure of 10 MPa, demonstrating that the gravity-free solution can indeed be used in an elastic model to retrieve pressure at depth from observed surface displacements when the reservoir geometry is known. As a third comparison, since Fig. 10 shows that a reservoir at depth in an elastic host can become pressurized to a significant extent above σ_z prior to

failure, if the same model geometry is retained and the pressure is raised until first failure occurs the resultant uplift is much greater, on the order of 0.25 m; it is worth noting that the uplift magnitude is effectively unchanged if higher values of the tensile strength (e.g., $T=5$ MPa) are used for the host rock. Based on current results, approximately 0.25 m will be the maximum inflation-derived uplift permissible prior to tensile failure and, presumably, relief of the magma pressure driving the uplift process. Other sources of uplift stemming from magmatic activity can also, of course, play a significant role (e.g., Bonafede, 1990; Castagnolo et al., 2001).

Since the amount of uplift observed at the surface is strongly dependent upon both geometrical and geological parameters, however, it is instructive to conduct a second test using an actual inflation event. The June 1984 uplift measured at Campi Flegrei caldera in Italy provides a suitable test, as the topography of the area is fairly flat and the event has recently been modeled using elastic and elasto-plastic FEM techniques by Trasatti et al. (2005). In

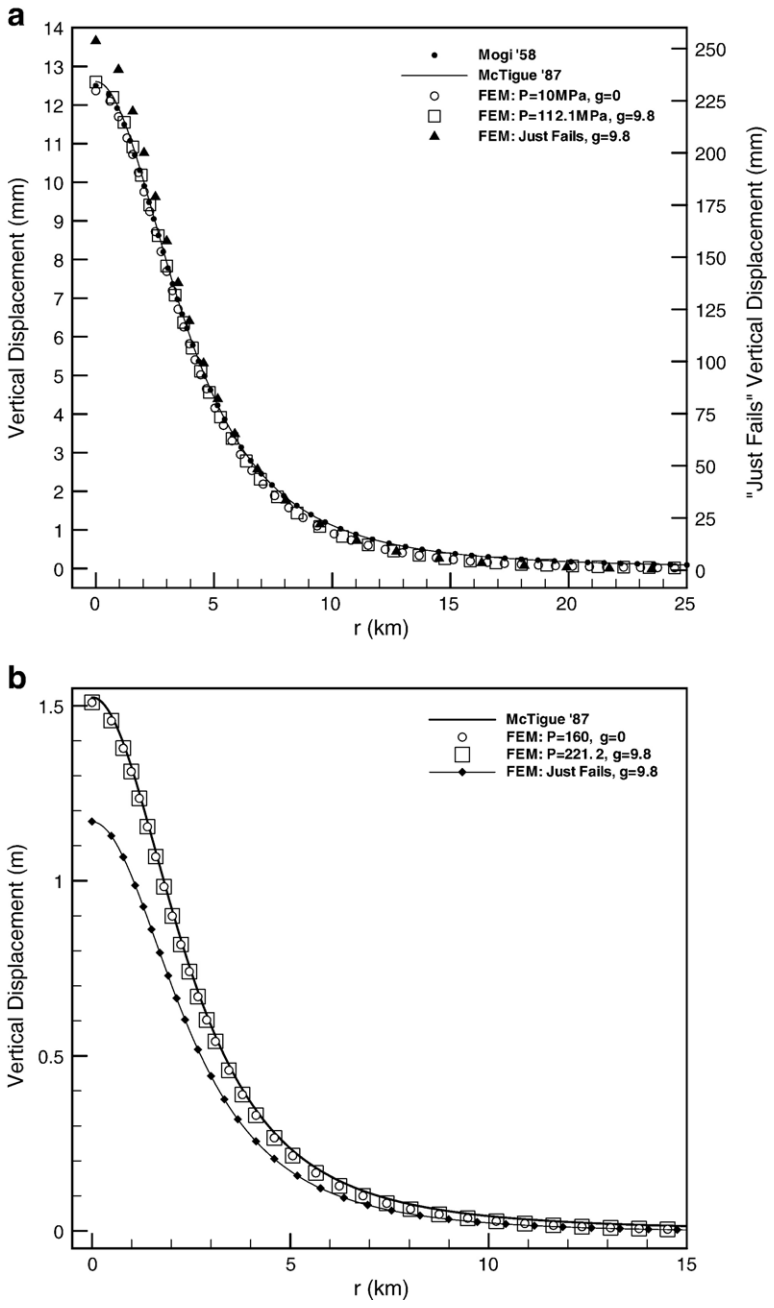

their Fig. 2, following McTigue (1987), Trasatti et al. (2005) show that the best fit analytical elastic solution to the field measurements of Berrino et al. (1984) and other available constraints is a sphere with $R=0.8$ km, DtC=3.2 km, $P_e=160$ MPa, $\nu=0.25$, and $G=4$ GPa. Fig. 14b plots the analytical prediction and compares it with several different numerical results from the current study. First, turning off gravity in the FEM results in uplift very close to but again very slightly less than that predicted using the McTigue (1987) model cited by Trasatti et al. (2005) as the best fit to the June 1984 Campi Flegrei caldera event. Second, using the same approach as in the 10 MPa excess pressure case explored previously, P is set to $\sigma_z(h=0)+P_e \approx 221.2$ MPa. This once again yields an excellent fit to the results Trasatti et al. (2005) obtain using the McTigue (1987) analytical model. As Trasatti et al. (2005) note, however, this excess pressure is quite high, and they claim that 160 MPa is a physically implausible value for the pressure as it will generate tensile stresses parallel to the reservoir wall of ~80 MPa (i.e., using Eq. (11)), comparable to the magnitude of the lithostatic stress, which is ~81.5 MPa at the DtC of the reservoir. For the geometry proposed, however, Fig. 10 shows that first failure will occur when $P=2.27\sigma_z \approx$ 185.1 MPa (with $z=$DtC); the net value of $P \approx 221.2$ MPa identified by Trasatti et al. (2005) is thus problematic, as they contend, but not for the quantitative reason they contend. Instead, the problem is that the pressure required to generate the observed surface uplift exceeds the maximum value of 185.1 MPa allowed for this elastic reservoir prior to initiation of tensile failure. When P is set to 185.1 MPa, yielding the maximum allowable uplift an elastic model of this geometric and geological configuration can support, the predicted uplift is ~30 cm less than the peak uplift value observed in the field. To first order this reinforces Trasatti el al.'s (2005) contention that a simple elastic model is unable to reproduce the uplift observed at Campi Flegrei in June of 1984. However, it augments the work by Trasatti et al. (2005) by redefining the upper bound for the magnitude of the pressure, and hence the magnitude of the uplift, which can be supported in an elastic treatment of the Campi Flegrei event using the reservoir geometry they propose.

Two important conclusions can be drawn from the uplift model comparisons performed above. First, the reservoir pressures inferred from (a) models which treat the reservoir as a pressurized sphere in an infinite (but unloaded) elastic medium, and (b) models which treat the reservoir as a pressurized body in a fully loaded host rock system, are identical. This is very different than the outcome when using these two styles of model to characterize the location of, and P sustainable prior to, reservoir failure. Second, before concluding that a simple elastic model fails to reproduce a particular uplift scenario, it is necessary to consider the pressure within the reservoir system very carefully. Fig. 10 places an upper bound on the pressure and hence uplift sustainable by a given reservoir geometry, thus establishing a new quantitative basis for evaluating whether or not a given amount of uplift observed in the field can indeed be explained using elastic models.

4.6. Magma pressure and failure

Fig. 10 demonstrates that, for an elastic system, a magma reservoir can support a wide range of uniform pressures P prior to the initiation of tensile failure. This result is certainly at odds with studies that claim failure will occur when P rises to at most only a few MPa above lithostatic (e.g., Blake, 1981; Gautneb et al., 1989; Tait et al., 1989; Gudmundsson, 1998, 2002; Pinel and Jaupart, 2003, 2004, 2005; Gudmundsson, 2006), and as argued earlier the difference stems predominantly from how gravity is incorporated into the model formulations. The value of P required to initiate failure of a reservoir within a gravitationally stressed system places a limit on

Fig. 14. Vertical displacement of the surface as a function of radial distance r from the point at the surface directly above the reservoir center ($r=0$) out to a distance r equal to roughly five times the reservoir DtC. (a) The well known and commonly employed solutions for surface displacement identified by Mogi (1958) and McTigue (1987), which identify uplift due to inflation of a uniformly pressurized reservoir in an elastic host, are plotted for $P=10$ MPa in a reservoir of radius $R=1$ km located at DtC=5 km. When the same conditions are duplicated in the FEM, with $g=0$ m s^{-2}, the analytical solution is well approximated (maximum difference<2%). For the same geometry, if gravity is included, a uniform pressure $P=112.1$ MPa is required to produce the same amount of surface displacement, which in this instance is ~12 mm; this is simply the lithostatic pressure at the crest of the sphere (~102 MPa) plus the stated 10 MPa overpressure. Since a full gravitational solution permits significantly higher pressures for this geometry prior to failure (see Fig. 10), however, setting P so that failure is first induced permits calculation of the maximum uplift that can be sustained by inflation of a reservoir in this type of elastic model, which in this case is ~250 mm. (b) Application to the 1982—1984 uplift event at Campi Flegrei. The best fit elastic solution, calculated by Trasatti et al. (2005) using the McTigue (1987) model with Poisson's ratio set to 0.25 and the shear modulus to 4 GPa, indicates that uplift resulted from inflation of a spherical reservoir with $R=0.8$ km, DtC=3.2 km, and $P=160$ MPa. For the same set of parameters, the finite element approach yields the same result if either $g=0$ m s^{-2} and $P=160$ MPa or, as in (a), P is set to the lithostatic value at the crest of the reservoir (~61.2 MPa) plus the overpressure (160 MPa). However, for the geometry proposed, the maximum pressure allowed without causing tensile failure is $P=2.27\ \sigma_z=185.1$ MPa, which is capable of generating only ~1.2 m of uplift, well below the ~1.5 m observed. An elastic solution using the reservoir geometry proposed is incapable of generating the necessary uplift before inducing an intrusion event; see text for details.

the amount of vertical surface displacement that can be generated without inducing an intrusive event. When the pressure required to model an uplift event exceeds this limit then the elastic model as formulated becomes internally inconsistent. As noted above, one possible solution when this occurs is to explore whether modifications to the model geometry or elastic parameters can reduce the pressure to acceptable values without violating known geological and geometric constraints for the system under study; Trasatti et al. (2005) demonstrate that this approach is often unsuccessful. A second possibility is to adopt a conceptually different failure criterion (e.g., Jellinek and DePaolo, 2003). For instance, most analytical and numerical models treat the reservoir as an ideal ellipsoid, but perhaps the reservoir walls are better characterized as jagged and cracked, and the pressure that should be sought is one capable of converting these existing flaws into active intrusions (e.g., Rubin, 1995a). A third possible solution when faced with an implausible value of P in a simple elastic model, the potential applicability of which to volcanic systems has been studied extensively, is to explore more complicated subsurface structures in an elastic regime (e.g., Bianchi et al., 1987; Chevallier and Verwoerd, 1988, 1990; Quareni, 1990; Gudmundsson, 2002; Trasatti et al., 2003) or to integrate non-elastic rheologies into the model (e.g., Bonafede et al., 1986; Dragoni and Magnanensi, 1989; Maeda, 2000; Trasatti et al., 2005).

Fig. 10 also demonstrates that, when $R/\mathrm{DtC}>0.625$ (i.e., $\mathrm{DtC}<1.6R$) the pressure required to induce failure is less than the lithostatic stress in the surrounding host rock. However, the magma itself has weight, and while Fig. 10 plots the uniform pressure P, the total internal pressure P_m within the magma system is described by Eq. (4). In order to assess whether inclusion of the magma weight plays an important role, it is straightforward to calculate P_m acting at each model's failure location by adding the pressure from the magma at the depth h where failure occurs. Qualitatively, recognizing that rupture is predicted to occur predominantly near the crest of the reservoir under lithostatic conditions, h will generally be small, and thus the stress contributed by the magma weight should be minimal. Quantitatively, after adding the magma load component, P_m remains less than the lithostatic value when $R/\mathrm{DtC}>0.67$ (i.e., $\mathrm{DtC}<1.5R$). This difference is minor, and furthermore the outcome is unaltered by the host rock density structure or magma density relative to the host for a geologically plausible range of conditions. Reservoirs with $\mathrm{DtC}<1.5R$ are thus fundamentally unstable at shallow depths on physical grounds, according to an elastic model as formulated here, because a state of pressure equilibrium with the surrounding rocks could not be achieved before failure would occur. Reservoirs at these depths could form, however, under conditions (e.g., rheological or tectonic) different from those explored in the current model.

4.7. Uniaxial strain conditions

While modeling host rock stresses resulting from uniaxial strain conditions is rarer than the use of a lithostatic state, a fairly detailed study of magma reservoirs under uniaxial strain conditions was performed by Sartoris et al. (1990), using a finite element numerical approach, for several different reservoir geometries, all of fairly equivalent volume (a sphere with $R=1.5$ km) at a fixed DtC (5.4 km). Using a uniform density host and a reservoir subjected to depth-dependent internal pressure P_m (i.e., Eq. (4)), their main conclusions are that: failure is localized at the poles of the reservoir; this localization occurs for spherical, prolate and oblate reservoirs and is thus independent of geometry; the stresses around the reservoir are unaffected by variations in the magma density; and, introducing gravity into the modeling process stabilizes the reservoirs, meaning that failure requires greater magma pressures than predicted by analytical models. Qualitatively, all of these conclusions are supported by the results from the current modeling effort.

Quantitatively, however, Sartoris et al. (1990) argue that the critical uniform pressure P required to induce tensile failure at the crest of a spherical reservoir (their definition requires exceeding $T=10$ MPa) is $\sim 0.5\rho_r g(\mathrm{DtC}-R)$, i.e. half the lithostatic stress value at the crest of the reservoir. This contention is not supported by the current model results, which indicate that failure will occur when P is at or close to zero for reservoirs of different shapes at a wide variety of depths. Duplicating Sartoris et al.'s (1990) spherical model geometry and conditions, and setting P equal to half the lithostatic stress value at the crest of the reservoir, the most tensile tangential stress, σ_θ, exceeds their failure criterion across $\sim 34°$ of arc (i.e., the area where $\alpha>56°$), commensurate with the region identified as failing by Sartoris et al. (1990). When $P=0$, however, the reservoir wall will still fail across $\sim 10°$ of arc. This difference is not trivial, but the key point is unaffected: as is the case for the $P<\sigma_z$ state discussed for lithostatic conditions, a spherical reservoir subjected to uniaxial strain conditions will not be stable because failure of the walls should occur well before pressure equilibrium with the surrounding rocks is achieved. If magma collects to form an ellipsoidal reservoir in uniaxial strain conditions, it suggests that non-elastic rheology or some other

factor not considered in the current models has played an important role in the process.

4.8. Radiating dike swarms

Radiating dike swarms are regularly observed elements of complex magmatic systems on several different planets (e.g., Head and Wilson, 1992; McKenzie et al., 1992; Grosfils and Head, 1994; Wilson and Head, 1994; Koenig and Pollard, 1998; Ernst et al., 2001; Grindrod et al., 2005). Considerable geological evidence suggests that the dikes within these radial systems often form through lateral propagation of magma away from source regions located at shallow depths in the crust (e.g., Muller and Pollard, 1977; Ernst and Baragar, 1992; Parfitt and Head, 1993; Chadwick and Dieterich, 1995; Ernst et al., 1995; Fialko and Rubin, 1999). Because the geometry of many systems suggests that the source region is circular or elliptical in plan view, most studies adopt a magma reservoir source consistent with this constraint.

After modeling a range of geological and geometrical conditions for the current study, it is important to recognize that no circumstances in the elastic model formulated here yield rupture of the reservoir walls in a fashion consistent with the initiation of lateral dikes. This result directly contradicts analytical model findings that lateral dike emplacement should be the norm for many reservoir systems (e.g., Parfitt et al., 1993), and the cause of the difference derives primarily from the full integration of gravitational loading effects in the current model.

If radiating dikes are not explained by models that depict magma reservoirs as ellipsoidal bodies in a homogeneous elastic host rock, where might such a model be falling short? Several obvious possibilities can be listed, none of which (to my knowledge) has yet to be tested exhaustively. First, some other failure criterion may be more appropriate than the tensile failure condition employed in the current model. If the rock surrounding the reservoir is treated as a heavily fractured mass, perhaps reactivation of cracks through Mohr–Coulomb-style mechanisms that rely on the net three-dimensional stress field adjacent to the reservoir would be more realistic. This could in turn create opportunities for magma to intrude existing flaws (e.g., as laid out in Rubin, 1995a), though why these would yield radiating suites of dikes and not other geometries would have to be addressed in a systematic fashion. A second possibility is that geological inhomogeneities, for instance loading due to the presence of a volcanic edifice, the presence of major faults, or variation in the properties of subsurface layers will affect the host rock stress state near the reservoir in an elastic model. Several recent efforts have explored these topics, most without focusing on constraining the nature of reservoir wall failure (e.g., Bianchi et al., 1987; Chevallier and Verwoerd, 1988, 1990; Chadwick and Dieterich, 1995; Saunders, 2001; Gudmundsson, 2002; Pinel and Jaupart, 2003, 2004; Russo and Giberti, 2004; Lungarini et al., 2005; Pinel and Jaupart, 2005; Trasatti et al., 2005). It is worth noting as well that many large, 'pristine' radiating dike systems are not associated with central topography (cf. Grosfils and Head, 1994), and any other inhomogeneities invoked must be present frequently in volcanic systems on multiple planets to provide a convincing mechanism for explaining lateral dike injection. A third possibility is that the process of intrusion by other bodies, for instance the circumferential features favored when a reservoir lies at shallow depth, will modify the local stress field in a fashion which facilitates lateral dike injection for some period of time thereafter. This sort of reservoir modeling has been performed with other goals in mind (e.g., deformation of the floor of Rabaul caldera; Saunders (2001)) but has not been used to test the effect on failure location and the ability to cause lateral dike injection. A fourth possibility is that models invoking non-elastic rheologies, for instance on thermal grounds, could alter the stresses surrounding a reservoir considerably (e.g., Bonafede et al., 1986; Dragoni and Magnanensi, 1989; Maeda, 2000; Newman et al., 2001; Jellinek and DePaolo, 2003; Trasatti et al., 2003, 2005). The goal of most non-elastic models has been to reproduce surface uplift or eruption patterns, but there has not yet been a directed effort to test the circumstances that will promote magma reservoir rupture under these conditions. A final obvious possibility is that the geometry of the reservoir may not be ellipsoidal. A "plexus of cracks" model (e.g., Takada, 1989) is unsatisfying as an explanation on physical grounds since it is not clear why stress states promoting lateral emplacement of any kind, little less into organized radial dike systems, would be favored; however, a planar elastic model of dike emplacement developed by Kühn (2005) demonstrates that dike focusing can create a reservoir-like cluster of dikes, and dikes rolled over into sills, that generates net stresses comparable to those expected around an elliptical reservoir, although once again stresses compatible with lateral dike generation are not indicated. Finally, other regular reservoir geometries should be considered, a path that has been explored extensively (e.g., Dieterich and Decker, 1975; Chevallier and Verwoerd, 1988; Yang et al., 1988; Chevallier and

Verwoerd, 1990; Chadwick and Dieterich, 1995). In many such efforts, however, problems related to those described earlier are introduced. To illustrate, Chadwick and Dieterich (1995) construct a finite element model of a pressurized reservoir in a stress-free host (configured like a Galapagos volcano) based on the argument that, with $\rho_r = \rho_m$, the depth-dependent loading terms cancel out and gravitational stresses can thus be eliminated. This is directly akin to the approach used in many analytical models, and as discussed above results in the loss of important information when constraining the stresses around the reservoir. No effort is made here to reproduce the surface topography and intriguing diapiric reservoir geometry favored by Chadwick and Dieterich (1995) as an explanation for the full suite of circumferential and radial intrusions observed in the Galapagos, but the results presented above indicate that the stress model they develop lacks elements that are most likely necessary when constraining both the intrusion styles and intrusion locations within the edifice.

5. Conclusions

Analytical and numerical models that treat magma reservoirs as internally pressurized ellipsoidal cavities within an elastic half space have been used extensively to gain insight into the behavior of magma plumbing systems. While arguably limited in their ability to simulate the complexity characteristic of volcanic areas, elastic models are nonetheless widely used to investigate magma reservoir phenomena directly and to calibrate the development of more advanced models that enhance our simulation capacities. It is thus critically important to ensure that elastic models provide an accurate representation of magma reservoir behavior. By incorporating all major geological and geometrical factors examined in previous studies, the finite element half-space model employed in the current work provides a framework within which differences between published elastic magma reservoir results can be explored, compared, and better understood. The model results are summarized in Section 3.6. Subsequent analysis, and comparison with previously published elastic models, indicate that differences between and problems with elastic models derive principally from a single, simple source: the role played by gravity.

The first important insight gained here is that gravitational loading plays a key role in a wide variety of magma reservoir phenomena, yet gravitational effects are often incorporated either incorrectly or incompletely into published analytical and numerical models of magma reservoir behavior. A magma reservoir cannot be treated as a sphere within an unloaded elastic medium subjected only to an internal overpressure, although this approach is often argued to be valid on the basis of a one-dimensional stress balance across the reservoir wall. Failure to incorporate gravitational loading fully, for example, affects inferences about the internal pressure that a reservoir can sustain prior to rupture, and the location and orientation at which rupture of the reservoir wall will occur. Running numerical models that incorporate full gravitational loading also proves advantageous when modeling surface uplift because quantitative constraints can be placed upon the maximum internal pressure that can be sustained prior to failure of the reservoir walls, and hence the maximum amount of uplift an elastic model is capable of explaining.

The second important insight gained is that the three dimensional nature of the host rock stress field must be considered fully when evaluating rupture, even for a criterion as simple as induced tensile failure of the reservoir wall. This problem commonly manifests in two distinct forms. First, extensional stresses parallel to the reservoir wall, induced by the normal stress balance acting across it, are resisted by wall-parallel lithostatic stress components within the host rock that vary with depth. A byproduct of the one-dimensional stress balance approach mentioned above, which is used to eliminate gravitational loading from many models, is that the role played by the wall-parallel stresses resisting tensile failure is ignored in the resulting treatment of the reservoir. This is a critical problem since the difference between the magnitudes of the host rock stresses across the vertical extent of the reservoir dwarfs any variations in tensile stress induced by depth-dependent density differences between the magma and host rock. An important outcome of retaining the resisting host rock stresses is that neither host rock nor magma density differences play much of a role in the location of failure, a result clearly at odds with many published elastic model results. The second way the host rock stress field problem manifests itself is in the orientation of failure. When examining stresses parallel to the wall of a spherical reservoir, many elastic derivations must equate the stresses acting within a horizontal plane (σ_θ) and those acting within a vertical plane (σ_t). This assumption is only valid, however, when the stresses acting upon the reservoir are neither depth-dependent nor modified by the proximity of the free surface. Since both factors affect a magma reservoir under normal circumstances, models seeking to constrain intrusion geometry can't do so unless both σ_θ and σ_t are calculated. To illustrate the resulting problem, many published models using a tensile failure criterion conclude that lateral dikes are readily generated in response to pressurization of a spherical reservoir centered at a level of

neutral buoyancy, when in fact failure near the middle of a spherical reservoir is not favored under any geologically plausible circumstances when a three dimensional host rock stress field is employed. Even when a reservoir is oblate, a geometry promoting failure at the correct location, lateral sills rather than dikes are favored because σ_t is the first stress to exceed the tensile strength of the host rock.

In spite of the importance of incorporating gravitational loads correctly, and considering their effects in a three dimensional sense, the final major insight gained here is that neither the relative pressure required to induce rupture nor the location of failure is affected if the gravitational acceleration g used in the model is changed from a standard Earth value to one characteristic of Mars. Fortuitously, since the values of P and α characterizing rupture in a given situation are also altered very little even by the most extreme but geologically plausible variations in the tensile strength, shear modulus, or host rock and magma density structures, the current model is effectively insensitive to material parameters which are not well constrained on other planets. As a result, provided that characterization of a magma reservoir as an inflated ellipsoid within an elastic medium is suitable, and that tensile rupture of the walls is the appropriate failure criterion to apply, the model developed here can be used to gain insight into not only magma reservoirs on Earth, but also those believed to have formed within the crust of Mars, Venus and other planets.

Acknowledgements

The ideas presented here were stimulated by discussions with many individuals, but Jim Head, Liz Parfitt, Marc Parmentier, Allan Rubin and Lionel Wilson deserve special thanks for generously sharing their insights into magma reservoir evolution and/or numerical modeling over the span of many years. An earlier version of this manuscript benefited from discussions with Richard Ernst, Patrick McGovern, David Pollard, Linda Reinen and Susan Sakimoto, and I am grateful for the insightful critiques provided by Eleonora Rivalta, Agust Gudmundsson and an anonymous reviewer. This work was supported in part by NASA grants NAG5-9618, NAG5-10498 and NNG05GJ92G.

References

Anderson, E.M., 1936. Dynamics of the formation of cone-sheets, ring-dykes, and cauldron-subsidences. Proceedings of the Royal Society of Edinburgh 56, 128–157.

Anderson, E.M., 1951. The Dynamics of Faulting and Dyke Formation with Applications to Great Britain. Oliver and Boyd, Edinburgh. 206 pp.

Berrino, G., Corrado, G., Luongo, G., Toro, B., 1984. Ground deformation and gravity changes accompanying the 1982 Pozzuoli Uplift. Bulletin of Volcanology 47 (2), 187–200.

Bianchi, R., et al., 1984. Modeling of surface ground deformations in the Phlegraean Fields volcanic area, Italy. Bulletin of Volcanology 47 (2), 321–330.

Bianchi, R., et al., 1987. Modeling of surface deformation in volcanic areas; the 1970–1972 and 1982–1984 crises of Campi Flegrei, Italy. Journal of Geophysical Research 92 (B13), 14,139–14,150.

Blake, S., 1981. Volcanism and the dynamics of open magma chambers. Nature 289, 783–785.

Bonafede, M., 1990. Axi-symmetric deformation of a thermo-poro-elastic half-space: inflation of a magma chamber. Geophysical Journal International 103, 289–299.

Bonafede, M., Dragoni, M., Quareni, F., 1986. Displacement and stress-fields produced by a center of dilation and by a pressure source in a viscoelastic half-space — application to the study of ground deformation and seismic activity at Campi-Flegrei, Italy. Geophysical Journal of the Royal Astronomical Society 87 (2), 455–485.

Castagnolo, D., Gaeta, F.S.D.N.G., Peluso, F.M.G., Troise, C.P.F., Mita, D.G., 2001. Campi Flegrei unrest episodes and possible evolution towards critical phenomena. In: De Natale, G., Kilburn, C., Chouet, B.A. (Eds.), 1998 meeting of the European Geophysical Society. Elsevier, pp. 13–40.

Chadwick, W.W., Dieterich, J.H., 1995. Mechanical modeling of circumferential and radial dike intrusion on Galapagos volcanoes. Journal of Volcanology and Geothermal Research 66 (1–4), 37–52.

Chevallier, L., Verwoerd, W.J., 1988. A numerical model for the mechanical behavior of intraplate volcanoes. Journal of Geophysical Research 93, 4182–4198.

Chevallier, L., Verwoerd, W.J., 1990. Influence of temperature on the distribution of stress and displacement in a volcano: a numerical approach. Bulletin of Volcanology 52, 413–425.

Dieterich, J.H., Decker, R.W., 1975. Finite-element modeling of surface deformation associated with volcanism. Journal of Geophysical Research 80 (29), 4094–4102.

Dragoni, M., Magnanensi, C., 1989. Displacement and stress produced by a pressurized, spherical magma chamber, surrounded by a viscoelastic shell. Physics of the Earth and Planetary Interiors 56, 316–328.

Ernst, R.E., Baragar, W.R.A., 1992. Evidence from magnetic fabric for the flow pattern of magma in the Mackenzie giant radiating dyke swarm. Nature 356, 511–513.

Ernst, R.E., Head, J.W., Parfitt, E., Grosfils, E.B., Wilson, L., 1995. Giant radiating dyke swarms on Earth and Venus. Earth-Science Reviews 39, 1–58.

Ernst, R.E., Grosfils, E.B., Mege, D., 2001. Giant dike swarms: Earth, Venus and Mars. Annual Review of Earth and Planetary Sciences 29, 489–534.

Fedotov, S.A., 1982. Temperatures of entering magma, formation and dimensions of magma chambers or volcanoes. Bulletin of Volcanology 45, 333–347.

Fialko, Y.A., Rubin, A.M., 1999. Thermal and mechanical aspects of magma emplacement in giant dike swarms. Journal of Geophysical Research 104 (B10), 23,033–23,049.

Gautneb, H., Gudmundsson, A., Oskarsson, N., 1989. Structure, petrochemistry and evolution of a sheet swarm in an Icelandic central volcano. Geological Magazine 126, 659–673.

Greenough, J.D., Hodych, J.P., 1990. Evidence for lateral magma injection in the early Mesozoic dykes of eastern North America. In:

Parker, A.J., Rickwood, P.C., Tucker, D.H. (Eds.), Mafic Dykes and Emplacement Mechanisms. A.A. Balkema Publishers, Rotterdam, pp. 35–46.

Grindrod, P.M., Nimmo, F., Stofan, E.R., Guest, J.E., 2005. Strain at radially fractured centers on Venus. Journal of Geophysical Research 110 (E12), E12002. doi:10.1029/2005JEE002416.

Grosfils, E.B., Head, J.W., 1994. The global distribution of giant radiating dike swarms on Venus: implications for the global stress state. Geophysical Research Letters 21, 701–704.

Gudmundsson, A., 1988. Effect of tensile stress concentration around magma chambers on intrusion and extrusion frequencies. Journal of Volcanology and Geothermal Research 35, 179–194.

Gudmundsson, A., 1998. Formation and development of normal-fault calderas and the initiation of large explosive eruptions. Bulletin of Volcanology 60 (3), 160–170.

Gudmundsson, A., 2002. Emplacement and arrest of sheets and dykes in central volcanoes. Journal of Volcanology and Geothermal Research 116, 279–298.

Gudmundsson, A., 2006. How local stresses control magma-chamber ruptures, dyke injections, and eruptions in composite volcanoes. Earth Science Reviews 79, 1–31.

Head, J.W., Wilson, L., 1992. Magma reservoirs and neutral buoyancy zones on Venus: implications for the formation and evolution of volcanic landforms. Journal of Geophysical Research 97, 3877–3903.

Jaeger, J.C., Cook, N.G.W., 1979. Fundamentals of Rock Mechanics. Chapman and Hall, New York. 593 pp.

Jeffery, G.B., 1921. Plane stress and plane strain in bipolar co-ordinates. Philosophical Transactions of the Royal Society of London, Series A 221, 265–293.

Jellinek, A.M., DePaolo, D.J., 2003. A model for the origin of large silicic magma chambers; precursors of caldera-forming eruptions. Bulletin of Volcanology 65 (5), 363–381.

Klein, F.W., Koyanagi, R.Y., Nakata, J.S., Tanigawa, W.R., 1987. The seismicity of Kilauea's magma system. U.S. Geological Survey Professional Paper 1350, 1019–1185.

Koenig, E., Pollard, D.D., 1998. Mapping and modeling of radial fracture patterns on Venus. Journal of Geophysical Research 103, 15183–15202.

Kühn, D., 2005. Numerical simulation of magma ascent by dykes and crust formation at spreading centres. PhD thesis, University of Hamburg, Germany.

Lister, J.R., Kerr, R.C., 1991. Fluid-mechanical models of crack propagation and their application to magma transport in dykes. Journal of Geophysical Research 96, 10049–10077.

Lungarini, L., Troise, C.M.M., De Natale, G., 2005. Finite element modeling of topographic effects on elastic ground deformation at Mt. Etna. Journal of Volcanology and Geothermal Research 144 (1–4), 257–271.

Maeda, I., 2000. Nonlinear visco-elastic volcanic model and its application to the recent eruption of Mt. Unzen. Journal of Volcanology and Geothermal Research 95 (1–4), 35–47.

McGarr, A., 1988. On the state of lithospheric stress in the absence of applied tectonic forces. Journal of Geophysical Research 93, 13609–13617.

McKenzie, D., McKenzie, J.M., Saunders, R.S., 1992. Dyke emplacement on Venus and on Earth. Journal of Geophysical Research 97, 15977–15990.

McTigue, D.F., 1987. Elastic stress and deformation near a finite spherical magma body: resolution of a point source paradox. Journal of Geophysical Research 92, 12931–12940.

Mogi, K., 1958. Relationships between the eruptions of various volcanoes and the deformations of the ground surfaces around them. Bulletin of the Earthquake Research Institute, University of Tokyo 36, 99–134.

Muller, O.H., Pollard, D.D., 1977. The stress state near Spanish Peaks, Colorado, determined from a dike pattern. Pure and Applied Geophysics 115, 69–86.

Newman, A.V., Dixon, T.H., Ofoegbu, G.I., Dixon, J.E., 2001. Geodetic and seismic constraints on recent activity at Long Valley Caldera, California; evidence for viscoelastic rheology. Journal of Volcanology and Geothermal Research 105 (3), 183–206.

Parfitt, E.A., Head, J.W., 1993. Buffered and unbuffered dike emplacement on Earth and Venus: implications for magma reservoir size, depth, and rate of magma replenishment. Earth, Moon, and Planets 61, 249–281.

Parfitt, E.A., Wilson, L., Head, J.W., 1993. Basaltic magma reservoirs: Factors controlling their rupture characteristics and evolution. Journal of Volcanology and Geothermal Research 55, 1–14.

Pinel, V., Jaupart, C., 2003. Magma chamber behavior beneath a volcanic edifice. Journal of Geophysical Research 108 (B2).

Pinel, V., Jaupart, C., 2004. Likelihood of basaltic eruptions as a function of volatile content and volcanic edifice size. Conduit processes during explosive basaltic eruptions; an introduction. Journal of Volcanology and Geothermal Research 137 (1–3), 201–217.

Pinel, V., Jaupart, C., 2005. Some consequences of volcanic edifice destruction for eruption conditions. Journal of Volcanology and Geothermal Research 145 (1–2), 68–80.

Quareni, F., 1990. Finite element deformation of an elastic, non-uniform medium produced by a dilating or pressurized magma chamber. Geophysical Journal International 101, 243–249.

Rubin, A.M., 1995a. Getting granite dikes out of the source region. Journal of Geophysical Research 100, 5911–5929.

Rubin, A.M., 1995b. Propagation of magma-filled cracks. Annual Review of Earth and Planetary Sciences 23, 287–336.

Rubin, A.M., Pollard, D.D., 1987. Origins of blade-like dikes in volcanic rift zones. U.S. Geological Survey Professional Paper 1350, 1449–1470.

Russo, G., Giberti, G., 2004. Numerical modeling of surface deformations on Mt. Vesuvius Volcano (Italy) in presence of asymmetric elastic heterogeneities. In: Civetta, L., Orsi, G., Patella, D. (Eds.), European Geophysical Society 2001 meeting. Elsevier, pp. 41–54.

Sartoris, G., Pozzi, J.P., Philippe, C., Le Mouel, J.L., 1990. Mechanical stability of shallow magma chambers. Journal of Geophysical Research 95 (B4), 5141–5151.

Saunders, S.J., 2001. The shallow plumbing system of Rabaul Caldera; a partially intruded ring fault? Bulletin of Volcanology 63 (6), 406–420.

Schultz, R.A., 1995. Limits on strength and deformation properties of jointed basaltic rock masses. Rock Mechanics and Rock Engineering 28 (1), 1–15.

Tait, S., Jaupart, C., Vergniolle, S., 1989. Pressure, gas content and eruption periodicity of a shallow, crystallizing magma chamber. Earth and Planetary Science Letters 92, 107–123.

Takada, A., 1989. Magma transport and reservoir formation by a system of propagating cracks. Bulletin of Volcanology 52, 118–126.

Timoshenko, S., Goodier, J.N., 1951. Theory of Elasticity. Engineering Societies Monograph. McGraw-Hill Book Company Inc., New York. 506 pp.

Trasatti, E., Giunchi, C., Bonafede, M., 2003. Effects of topography and rheological layering on ground deformation in volcanic regions. Journal of Volcanology and Geothermal Research 122 (1–2), 89–110.

Trasatti, E., Giunchi, C., Bonafede, M., 2005. Structural and rheological constraints on source depth and overpressure estimates

at the Campi Flegrei caldera, Italy. Journal of Volcanology and Geothermal Research 144 (1–4), 105–118.

Turner, J.S., Campbell, I.H., 1986. Convection and mixing in magma chambers. Earth-Science Reviews 23, 255–352.

Wilson, L., Head, J.W., 1994. Mars: review and analysis of volcanic eruption theory and relationships to observed landforms. Reviews of Geophysics 32, 221–263.

Yang, X.-M., Davis, P.M., Dieterich, J.H., 1988. Deformation from inflation of a dipping finite prolate spheroid in an elastic half-space as a model for volcanic stressing. Journal of Geophysical Research 93, 4249–4257.